

Highlights

Energy-Carbon Pricing-Guided Collaborative Optimization for Local Integrated Energy Communities with Multi-Vector Electrification Consumers

Yufei Xi,Lujie Zuo,Meng Chen,Jiansheng Zhang,Lin Cheng,Ioannis Lestas

- A novel integrated energy community framework with multi-vector electrification consumers is designed.
- An energy-carbon pricing-guided strategy is proposed to optimize market trading.
- A collaborative optimization model based on a Nash bargaining game is developed for coordinated operations.
- Benefits of CO₂ reduction and chemical production in the electrochemical process are quantified.
- The impact of electrification consumer compositions on IEC performance is analyzed.

Energy-Carbon Pricing-Guided Collaborative Optimization for Local Integrated Energy Communities with Multi-Vector Electrification Consumers

Yufei Xi^a, Lujie Zuo^b, Meng Chen^{c,*}, Jiansheng Zhang^b, Lin Cheng^a and Ioannis Lestas^c

^aState Key Laboratory of Power System Operation and Control, Tsinghua University, Beijing, 100084, China

^bDepartment of Energy and Power Engineering, Tsinghua University, Beijing, 100084, China

^cDepartment of Engineering, University of Cambridge, Cambridge, CB2 1PZ, UK

ARTICLE INFO

Keywords:

Integrated energy community
Electrification consumers
Energy-carbon pricing
Electric Vehicle
Electrochemical park
Nash bargaining game

ABSTRACT

The integration of multi-energy services and CO₂ reduction measures is crucial for advancing the transition to low-carbon energy. This study proposes a novel Integrated Energy Community (IEC) framework that synergizes Electric Vehicles (EVs), Power-to-Chemical (P2C), and Power-to-Heat (P2H) electrification consumers to optimize renewable energy utilization and carbon management. The framework incorporates Electrochemical CO₂ Reduction (ECO2R) and Carbon Capture and Storage (CCS) technologies, enabling carbon trading and chemical product commercialization. Meanwhile, an energy-carbon pricing-guided collaborative optimization model is developed, utilizing Nash bargaining game theory to coordinate electricity, gas, and heat operations under limited communication. Case studies validate the model's effectiveness, with numerical results demonstrating its superior performance in operational efficiency, renewable energy utilization, and carbon reduction compared to conventional community systems.

1. Introduction

Extreme climate changes and ambitious decarbonization goals are major ongoing drivers of clean electricity growth and energy system reform [1]. By 2023, advancements in solar and wind power technologies helped Renewable Energy (RE) reach a record 30% share of global electricity generation [2]. As RE penetration rises, modern energy systems must maintain a supply-demand balance while enhancing flexibility to handle RE's inherent volatility. The local Integrated Energy Community (IEC) allowing cooperation and complementarity among diverse energy subsystems, has emerged as a prime platform for developing and utilizing flexibility resources. Moreover, as crucial carriers of a sustainable energy society, local IECs urgently require operational models that balance economic and environmental benefits to fulfill their social responsibility in reducing carbon emissions [3].

To improve RE accommodation, researchers have explored solutions to enhance system flexibility across various aspects. On the source side, the power supplier has expanded beyond traditional thermal units to include rapidly dispatchable generation facilities such as natural gas plants [4], pumped storage power stations [5], and Combined Heat and Power (CHP) units with bypass [6]. These flexible sources, with fast startup capabilities, help mitigate disruptions from intermittent RE, peak loads, and unexpected events, ensuring a reliable power supply. Another effective source-side approach is to increase the diversity and geographic coverage of local RE distributed generation [7]. For instance, Texas leverages wind and solar resources from two regions to supply electricity aligned with complementary demand curves [8]. Similarly, Taiyuan combines medium and high temperature solar thermal generation with Wind Turbines (WTs) in an IEC to create smoother RE output through their coordinated operation [9].

On the load side, the network interconnection of IECs extends traditional Demand Response (DR) beyond the electricity sector, providing consumers with multiple options to meet their energy needs. Electrification at the consumption end accelerates the adoption of market-competitive electric energy substitution technologies, transforming the load side from a passive role to an active participant in the energy system. In transportation, Electric Vehicles (EVs) can perform

*Corresponding author

✉ xyfneepu@outlook.com (Y. Xi); lujiezuo@gmail.com (L. Zuo); mc2545@cam.ac.uk (M. Chen); zhang-jsh@tsinghua.edu.cn (J. Zhang); chenglin@mail.tsinghua.edu.cn (L. Cheng); icl20@cam.ac.uk (I. Lestas)

ORCID(s): 0000-0002-7473-2939 (Y. Xi); 0009-0001-3968-6906 (L. Zuo); 0000-0002-4331-2907 (M. Chen); 0000-0002-8559-9184 (J. Zhang); 0000-0002-6868-1493 (L. Cheng); 0000-0002-7739-949X (I. Lestas)

valley-filling operations in response to dispatch commands. Al-Bahrani et al. [10] shifted the charging load of 30,000 EVs to low-price periods, using them as a DR resource to manage peak loads and optimize economic benefits. Li et al. [11] designed a multi-functional dispatching system that integrates thermal and RE power plants, EV clusters, and grid users, demonstrating the effectiveness of EVs in regulating peak loads and enhancing RE accommodation. In heating, “Power-to-Heat (P2H)” applications have gained significant attention. Proponents suggest that the heating network deserves higher priority at the local electricity consumption end, given that Thermal Energy Storage (TES) is often more cost-effective than Electric Energy Storage (EES) [12]. With P2H technologies such as electric boilers (EBs), heat pumps (HPs), and air conditioning systems, heat loads can serve as flexible and controllable power demand, efficiently using surplus RE electricity. For example, Zhou et al. [13] developed a DR control model based on temperature and load distribution, demonstrating the load regulation potential of HPs. Chen et al. [14] explored the DR potential of combined Photovoltaic (PV) and HP technologies, achieving a 13.8% reduction in operating costs through optimal scheduling in price- and incentive-based DR. Cai et al. [15] proposed a back propagation neural network-based method to assess central air-conditioning loads, highlighting the load adjustment capacities of air-conditioning systems in different industries. Notably, TES technology is commonly integrated into P2H applications, enabling the heat storage capacity to be shared with the power system through network interconnection.

Recently, burgeoning electrochemical technologies have broken the barriers between the chemical and electricity sectors. The “Power-to-Chemicals (P2C)” approach offers a longer-term and larger-scale solution to RE accommodation, while also providing new opportunities for the slow and costly decarbonization of traditional industries. Hydrogen production through water electrolysis has been extensively studied, with several technologies successfully commercialized [16], [17]. Another notable and emerging P2C application is Electrochemical CO₂ Reduction (ECO2R). ECO2R uses low-grade RE electricity to reduce CO₂ to produce high-value chemicals or fuels, such as carbon monoxide, formic acid, methanol, ethanol, ethylene, etc. [18]. Given its ability to absorb RE, an ECO2R park could serve as a new dispatchable electricity demand, improving system flexibility when deployed on the power load side. Manuel et al. [19] proposed a power-to-gas hybridization park that integrates electrochemical industries, where CO₂ for methanation can be captured from the flue gas of boilers without additional energy penalty. Zhang et al. [20] proposed a model combining carbon capture power plants with P2G technology, using surplus RE electricity and CO₂ emissions from the integrated system to enhance gas supply, providing a new approach to utilizing CO₂ instead of storing it. Lee et al. [21] proposed a RE system with an ECO2R park improving economic benefits by selling reduction products. Their optimization results demonstrated the commercial applicability of the ECO2R park, with methanol sales generating \$550/ton in revenue.

The above work highlights two key aspects in developing flexibility resources from a system composition perspective. First, it emphasizes fully leveraging the diversity and complementarity of generation facilities on the source side. Second, it focuses on increasing the electrification level of the load side. Meanwhile, researchers have argued that the local market plays a crucial role in the optimal allocation of flexibility resources in IECs. Through appropriate local market pricing signals, different subsystems can collaborate and optimize the management of various response resources, ultimately improving the performance and benefits of the entire IEC.

Some market pricing strategies are designed for centralized operation optimization, assuming that a central entity, such as an integrated system operator (ISO), is responsible for the unified management of energy subsystems. For example, Li et al. [22] proposed a Stackelberg game-based optimization framework to coordinate integrated DR and multiple RE generators, balancing the interests of the ISO and consumers. Similarly, Yang et al. [23] developed a bi-level model using Stackelberg game theory, where the upper level optimizes electricity prices and the lower level manages various types of flexible loads. Their dynamic pricing strategy effectively encouraged market participation from the flexible load side, enhancing RE integration and reducing energy costs. Tan et al. [24] proposed a robust dispatch model for an integrated electricity and heat system with price-based integrated DR. Their simulation results showed that appropriate electricity and heat pricing significantly improved local wind power accommodation. However, in reality, there is significant individual rationality and autonomy among operators across different energy sectors. In a competitive market, each operator is responsible for its own planning and operation, often with divergent or even conflicting objectives. To address this issue, the Nash bargaining game framework has been employed to optimize the collective performance of the system, while ensuring that the profits resulting from cooperation are fairly distributed among the involved parties. Xi et al. [25] proposed a Nash equilibrium market optimization model for an integrated gas-electricity-heat system with multiple flexible resources, improving total social welfare while optimizing RE accommodation. Li et al. [26] developed a Nash bargaining collaborative optimization model for a rural hybrid RE system that includes a CHP system, a biomass gas supply system, and an agricultural consumption system, achieving

an equitable distribution of value-added benefits in the circular economy among participants. Wang et al. [27] proposed a joint robust optimization model for long-term capacity planning and short-term operational strategies. Case studies involving the uncertainty of three energy hubs demonstrated that the asymmetrical bargaining solution can both effectively reduce the system cost and facilitate a fair benefit distribution.

These publications focus on economic-oriented operation models, with limited consideration of the environmental impacts of energy production and its effects on downstream industries. Several recent studies have introduced low-carbon objectives into operating models to align with decarbonization policies. For instance, Huang et al. [28] developed a low-carbon economic dispatch and energy-sharing framework based on the efficient utilization of regional carbon quotas, improving both operating costs and carbon quota distribution under strict emission constraints. Wang et al. [29] integrated carbon emission intensity into the multi-energy pricing process by tracing embedded carbon emissions. Yang et al. [30] proposed a carbon-energy integrated pricing strategy for seaport consumers, allowing them to adjust their consumption behaviors to optimize benefits and reduce carbon emissions. On this basis, Ma et al. [31] proposed a two-stage optimization model for energy hubs with nodal integrated energy-carbon pricing, effectively reducing both carbon emissions and operating costs by analyzing the impact of nodal prices on consumption patterns. Dai et al. [32] developed a two-stage distributed robust optimization model for multi-energy systems under PV output uncertainty and a ladder carbon trading mechanism, achieving a 5.54% reduction in carbon emission costs while balancing economic and environmental objectives.

Although these studies have incorporated carbon emission factors into cost optimization problems, few have effectively integrated carbon constraints with multi-energy interactions and pricing stages. Furthermore, these optimization strategies for both economic and low-carbon operations often overlook the coordination and interaction of various electrification consumers, particularly the market potential of P2C in achieving both economic and environmental benefits. To fill these gaps, this study develops a novel energy-carbon pricing-guided collaborative optimization model for a local IEC, enabling both cost-effective energy supply and market-competitive carbon emission reduction. The model enhances system flexibility by integrating Multi-Vector electrification consumers of the IEC, including EV clusters, P2H, and P2C, alongside storage facilities like Gas Energy Storage (GES) and TES, which can be shared through local network interconnection. Different from previous work [20] and [21], this paper emphasizes the downstream market of P2C, selling the various chemical products produced in its Electrochemical Park (EP) to the chemical industry to generate additional revenue. In the local market pricing stage, the marginal carbon tax is introduced into gas and electricity pricing strategies by tracing embedded carbon emissions from fuel combustion. In the energy management stage, each subsystem operator optimizes its own energy schedules/consumption behaviors based on the energy transaction prices. The key contributions of this study are as follows.

- (1) A novel local IEC framework integrating multi-vector electrification consumers is constructed. This framework enables electricity demand to align with RE generation effectively, and captures CO₂ from carbon-emitting producers, creating a closed-loop system for multi-energy-carbon coupling.
- (2) An energy-carbon pricing-guided strategy is proposed to coordinate responsive consumers and storage resources within the IEC. In the local market-based pricing stage, this strategy incorporates carbon-related constraints (carbon taxes and carbon emission trading prices) with multi-energy interactions from both source and load sides.
- (3) A collaborative optimization model based on the Nash bargaining game is developed for the IEC energy management. This model fosters a fair-competitive and self-interested market environment for subsystem operators.
- (4) Six cases with different compositions of electrification consumers are simulated and analyzed to assess the proposed IEC across four key aspects: pricing results, performance improvement, power demand reshaping, and flexibility services.

2. Framework and modeling

Fig. 1 illustrates the framework of the proposed IEC, depicting energy-carbon flows among the Natural Gas Subsystem (NGS), the Power Subsystem (PS), and the District Heating Subsystem (DHS). In this framework, energy units within the IEC are classified as producers, prosumers, consumers, or storage resources, depending on their market roles. Considering heat as a welfare product derived from the consumption of gas and electricity, the correspondence between market roles and system components is detailed in Table 1.

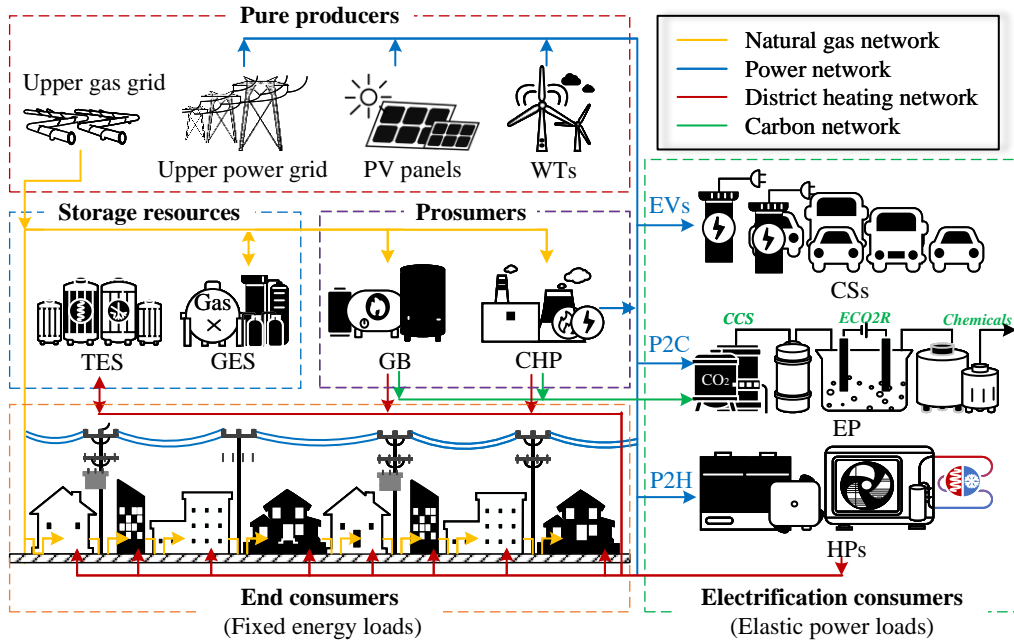


Figure 1: Framework of the proposed IEC.

Table 1

Correspondence between market roles and system components.

Energy Units	Managed by	Market roles	Supplementary explanation
Upper gas grid	NGS operator	Pure producer	External fossil fuel (gas) source for the entire IEC
Upper power grid	PS operator	Pure producer	External fossil fuel (power) source for the entire IEC
PV generation	PS operator	Pure producer	External RE (wind) source for the entire IEC
WTs	PS operator	Pure producer	External RE (solar) source for the entire IEC
GB	DHS operator	Prosumer	Gas consumer while heat producer
GFCHP	DHS operator	Prosumer	Gas consumer while heat and power producers
Gas load	NGS operator	End consumer	Gas consumer with fixed consumption pattern
Power load	PS operator	End consumer	Electricity consumer with fixed consumption pattern
Heat load	DHS operator	End consumer	Heat consumer with fixed consumption pattern
CSs	PS operator	Electrification consumer	Electricity consumer with elastic consumption pattern
EP	PS operator	Electrification consumer	Electricity consumer with elastic consumption pattern
HPs	DHS operator	Electrification consumer	Flexible electricity consumer while heat producer
GES	NGS operator	Storage resource	Charging/discharging gas for supply-demand balance
TES	DHS operator	Storage resource	Charging/discharging heat for supply-demand balance

The upper gas and power grids serve as reliable supply sources with sufficient capacity to ensure stable energy provision for the IEC during extreme RE fluctuations and peak demand. To enhance electricity demand flexibility, the IEC incorporates three electrification technologies: EV Charging Stations (CSs), P2C through the EP, and P2H using HPs. The EP, powered by surplus RE electricity, utilizes the Carbon Capture and Storage (CCS) system to capture CO₂ emissions from the Gas Boiler (GB) and the Gas-Fired Combined Heat and Power (GFCHP) unit, converting them into marketable chemicals via the ECO2R process. Strategically, the EP is located near the GB and GFCHP units to provide convenience for the CCS deployment.

Fig. 2 describes the interaction between subsystem operations within the IEC and local market procedures. Market participants—including energy producers, storage resources, and responsive consumers—submit external features such as economic and environmental cost functions, operational constraints, conversion efficiencies, and network parameters to their respective subsystem operators. An integrated balance responsible party coordinates local gas and electricity market procedures, ensuring equilibrium between energy sales and purchases during the bidding process. Based on

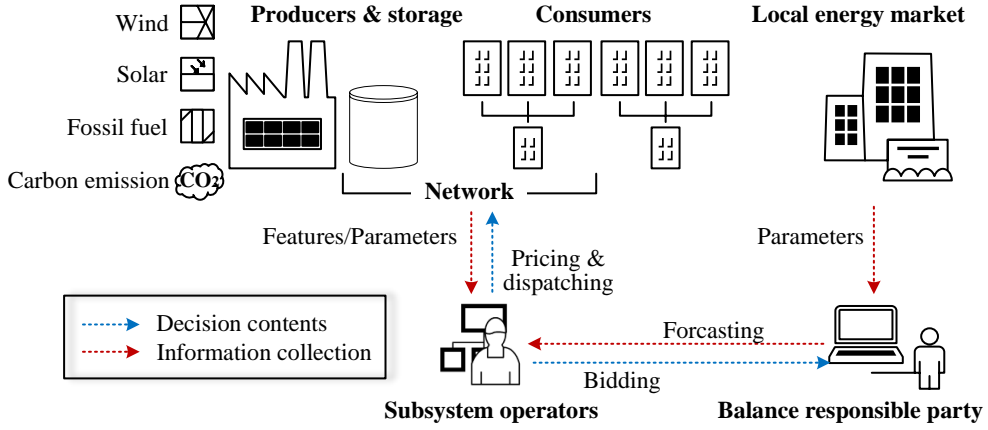


Figure 2: Interaction between subsystem operations and market procedures.

market outcomes and network losses, subsystem operators develop optimized dispatch strategies, issuing commands to align energy production and consumption within the IEC. The mathematical models of these market participants are detailed below.

2.1. Pure producers

2.1.1. RE power generation

PV power generation is influenced by solar radiation intensity, incident angle, and ambient temperature. The power output of PV panels can be expressed as [33]:

$$p_{i,t}^S = \frac{I_\theta}{1000} p_i^S \eta^S \cdot [1 + \gamma^S (T^a + \beta I_\theta - T^{\text{ref}})] \quad (1)$$

where, $p_{i,t}^S$ is the actual power generation of the PV station; $I_\theta/1000$ is the number of solar peak hours; p_i^S is the rated power of the PV array (kW); η^S expresses system efficiency; γ^S and β are the power temperature coefficient and variation coefficient of component temperature with radiation, respectively; T^a and T^{ref} are the ambient temperature and the reference ambient temperature, respectively ($^\circ\text{C}$).

The WT power generation depends on wind speed and turbine parameters, which can be expressed as [34]:

$$p_{i,t}^W = \begin{cases} 0 & (v_{i,t} \leq v^{\text{in}}, v_{i,t} \geq v^{\text{out}}) \\ f(v_{i,t}) & (v^{\text{in}} \leq v_{i,t} \leq v^{\text{rate}}) \\ p_i^W & (v^{\text{rate}} \leq v_{i,t} \leq v^{\text{out}}) \end{cases} \quad (2)$$

where, $p_{i,t}^W$ is the actual WT power generation (kW); $f(v_{i,t})$ is the fitting polynomial provided by the fan manufacturer; p_i^W is the rated output power of WT i (kW); $v_{i,t}$, v^{in} , v^{out} , and v^{rate} are the actual wind speed, cut-in wind speed, cut-out wind speed, and rated wind speed, respectively (m/s).

2.1.2. Upper energy grids

It is assumed that electricity from the upper power grid is supplied by large thermal power plants. For these plants, coal consumption depends on their peak-shaving operations. The relationship between coal consumption and power output can be described as [35]:

$$m_{i,t}^{\text{UPG}} = \begin{cases} bg \cdot p_{i,t}^{\text{UPG}} & (p_{i,\text{min}}^{\text{UPG}} \leq p_{i,t}^{\text{UPG}} \leq p_{i,\text{max}}^{\text{UPG}}) \\ f(p_{i,t}^{\text{UPG}}) & (p_{i,\text{dmin}}^{\text{UPG}} \leq p_{i,t}^{\text{UPG}} \leq p_{i,\text{min}}^{\text{UPG}}) \end{cases} \quad (3)$$

where, $m_{i,t}^{\text{UPG}}$ and $p_{i,t}^{\text{UPG}}$ are the coal consumption (kg) and power output (kW) of thermal power plant i , respectively; bg is the coal consumption rate (kg/kW); $p_{i,dmin}^{\text{UPG}}$, $p_{i,min}^{\text{UPG}}$, and $p_{i,max}^{\text{UPG}}$ are the minimum output for deep peak-shaving, the lower limit of the thermal power output, and the upper limit of the thermal power output, respectively (kW). In the basic peak-shaving range [$p_{i,min}^{\text{UPG}}$, $p_{i,max}^{\text{UPG}}$], the coal consumption rate remains relatively constant. Conversely, in the deep peak-shaving range [$p_{i,dmin}^{\text{UPG}}$, $p_{i,min}^{\text{UPG}}$], the coal consumption rate exhibits nonlinear behavior, decreasing rapidly as power output increases.

This study considers the upper gas grid as an infinite gas source. The steady-state modeling of the local gas network within the IEC is detailed in Section 3.

2.2. Prosumers

2.2.1. GB unit

GBs consume natural gas to produce heat, offering ease of installation and fast response times. The mathematical model can be simplified using linear expressions [36]:

$$q_{i,t}^{\text{GB}} = \eta^{\text{GB}} g_{i,t}^{\text{GB}} \quad (4)$$

$$q_{i,min}^{\text{GB}} \leq q_{i,t}^{\text{GB}} \leq q_{i,max}^{\text{GB}} \quad (5)$$

where, $q_{i,t}^{\text{GB}}$ and $g_{i,t}^{\text{GB}}$ are the hourly heat production and gas consumption of the GB, respectively (kW); η^{GB} is the conversion efficiency; $q_{i,min}^{\text{GB}}$ and $q_{i,max}^{\text{GB}}$ define the minimum and maximum thermal power outputs of GB unit i , respectively (kW).

2.2.2. GFCHP unit

GFCHP units produce electricity by burning natural gas while recovering the waste heat from turbines or engines for thermal applications. The relationships among electricity generation, heat production, and natural gas consumption can be expressed using linear equations [9]:

$$\begin{cases} q_{i,t}^{\text{GFCHP}} = \eta^{\text{gth}} g_{i,t}^{\text{GFCHP}} \\ p_{i,t}^{\text{GFCHP}} = \eta^{\text{gte}} g_{i,t}^{\text{GFCHP}} \\ \eta^{\text{gth}} = \eta^{\text{HE}} \cdot (1 - \eta^{\text{gte}} - \eta^{\text{L}}) \end{cases} \quad (6)$$

where, $g_{i,t}^{\text{GFCHP}}$, $p_{i,t}^{\text{GFCHP}}$, and $q_{i,t}^{\text{GFCHP}}$ are the gas consumption, electricity production, and heat production of the GFCHP unit, respectively (kW); η^{gth} , η^{gte} , η^{HE} , and η^{L} are the conversion efficiencies from gas to heat and gas to power, the heat exchange coefficient, and the heat loss coefficient, respectively. Furthermore, the operation of the GFCHP unit is subject to constraints on its electric power output and climbing capabilities.

$$q_{i,min}^{\text{GFCHP}} \leq q_{i,t}^{\text{GFCHP}} \leq q_{i,max}^{\text{GFCHP}} \quad (7)$$

$$\left| p_{i,t}^{\text{GFCHP}} - p_{i,t-1}^{\text{GFCHP}} \right| \leq p_{i,Climb}^{\text{GFCHP}} \quad (8)$$

where, $q_{i,min}^{\text{GFCHP}}$ and $q_{i,max}^{\text{GFCHP}}$ define the minimum and maximum electric power outputs of GFCHP unit i , respectively (kW); $p_{i,Climb}^{\text{GFCHP}}$ is the climbing limit of GFCHP unit i (kW).

2.3. Multi-vector electrification consumers

2.3.1. EV CSs

The local PS operator requires responsive EV clusters to adjust their charging schedules—either advancing or delaying them—according to dispatch commands. Assuming that the local IEC has N_t^{EV} dispatchable EV, each with a charging power of p^{EV} during period t , the flexible electricity demand of local CS i (kW) can be expressed as:

$$\begin{cases} p_{i,t}^{\text{CS,c}} = N_t^{\text{EV}} p^{\text{EV}} \\ p_{i,t}^{\text{CS,d}} = -N_t^{\text{EV}} p^{\text{EV}} \end{cases} \quad (9)$$

where, $p_{i,t}^{\text{CS,c}}$ represents the increased demand of CS i as N_t^{EV} EVs are instructed to advance their original charging plans to period t , while $p_{i,t}^{\text{CS,d}}$ indicates the decreased demand of CS i as N_t^{EV} EVs are instructed to delay their original charging plans from period t to other periods. Considering daily travel needs, the charging requirements of each EV must be fulfilled within 24 hours.

$$\sum_{t=1, I=1}^{T, I^{\text{CS}}} \left(p_{i,t}^{\text{CS,c}} - p_{i,t}^{\text{CS,d}} \right) = 0 \quad (10)$$

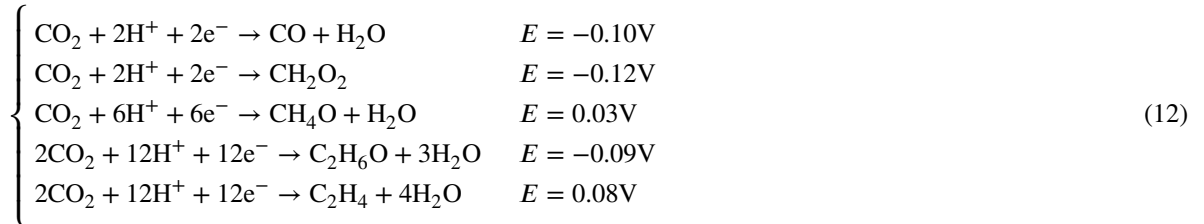
where, $T=24$ hours define the set of scheduling periods, and I^{CS} denotes the number of available CSs within the local IEC. Additionally, as part of the overall power load, each CS must adjust its demand according to dispatch commands while maintaining the safety and stability of the load-side network. The factor γ is introduced to represent the acceptable responsive-load ratio of the local PS. The hourly dispatchable demand of local CSs is limited by:

$$\left| \sum_{i=1}^{I^{\text{CS}}} p_{i,t}^{\text{CS,c}}, \sum_{i=1}^{I^{\text{CS}}} p_{i,t}^{\text{CS,d}} \right| \leq \gamma p_t^{\text{L}} \quad (11)$$

where p_t^{L} is the hourly power load of the IEC (kW).

2.3.2. EP based on CCS and ECO2R

The local PS operator utilizes P2C technology to efficiently consume surplus RE power through the EP. The production chain of the EP consists of two main steps: CCS and ECO2R. In the CCS process, an alkaline amine absorbent is used to capture CO_2 from the flue gas emitted by GB and GFCHP units. The captured CO_2 is then enriched and directed into an electrolyzer, where it is activated by a catalyst and converted into valuable chemicals. The ECO2R reaction within the electrolyzer can be described as follows [37]:



where E represents the bias potential applied to the electrolyzer (V vs. Reversible Hydrogen Electrode). It is worth noting that this study excludes natural gas (CH_4) as a reaction product due to its market value being less competitive compared to the above chemicals. In addition, the competitive hydrogen evolution reaction in the aqueous reduction environment should also be considered. This side reaction is shown as:



In the ECO2R process, the selectivity of chemical products is influenced by the applied potential E , catalysts, and electrolyte composition. The Faraday efficiency quantifies the ratio between the chemical product and the amount of charge required, reflecting the probability of generating the specific product. The Faraday efficiency is defined as [38]:

$$\eta^{\text{F}} = \frac{nNF}{I \cdot \Delta\tau} \times 100\% \quad (14)$$

where, n is the number of electrons transferred for different products; N is the molar number of the product (mol); F is Faradaic constant (96485 C/mol); I is the total current in the electrolyzer (A) and $\Delta\tau$ is the electrolysis time (s). According to the law of conservation of charge, the sum of the Faradaic efficiencies for all products must equal 1.

$$\sum_{j \in J} \eta_j^{\text{F}} = 1 \quad (15)$$

Table 2

Maximum Faraday efficiencies for different ECO2R products.

ECO2R product	n	Maximum FE	Refer to
Carbon monoxide (CO)	2	100%	[39]
Formic acid (CH ₂ O ₂)	2	96%	[40]
Methanol (CH ₄ O)	6	40%	[41]
Ethanol (C ₂ H ₆ O)	12	70%	[42]
Ethylene (C ₂ H ₄)	12	85%	[43]
Hydrogen (H ₂)	2	100%	[44]

where $J = \{CO, CH_2O_2, CH_4O, C_2H_6O, C_2H_4, H_2\}$.

Drawing from recent research advancements, Table 2 presents the theoretical maximum Faraday efficiency achievable for each product. The EP, driven by surplus RE electricity, offers both economic and environmental benefits to the local IEC: (1) Selling chemical products from the EP to downstream industries generates additional economic revenue, and (2) trading the carbon emissions reduced by the EP in the local carbon market provides environmental income. Accordingly, the chemical production and CO₂ reduction of the EP during period t are expressed as:

$$m_t^{CP} = \sum_{j \in J} \alpha^{EP} \eta_j^{CP} \eta_j^F \cdot \left(\sum_{i \in I^{WT}} p_{i,t}^{WT,S} + \sum_{i \in I^{PV}} p_{i,t}^{PV,S} \right) \Delta t$$

$$m_t^{CO_2} = \sum_{j \in J} \frac{Mr_{CO_2} \eta_j^{CP} \eta_j^F}{Mr_j} \cdot \left(\sum_{i \in I^{WT}} p_{i,t}^{WT,S} + \sum_{i \in I^{PV}} p_{i,t}^{PV,S} \right) \Delta t \quad (16)$$

where, m_t^{CP} is the total amount of chemicals produced by the EP (kg); $m_t^{CO_2}$ is the amount of CO₂ emissions consumed by the EP (kg); α^{EP} is the conversion factor of the EP investment cost; η_j^{CP} is the maximum conversion efficiency of product j (kg/kWh); Mr_{CO_2} and Mr_j are the molar mass of CO₂ and product j , respectively (kg/mol); $I^{WT/PV}$ denotes the number of operational WTs or PV panels within the local IEC; $p_{i,t}^{WT/PV,S}$ is the surplus RE power generated by WT/PV panel i during period t .

2.3.3. HP unit

The local DHS operator converts the heat demand into dispatchable electricity demand using HPs, helping the PS alleviate the mismatch between supply and demand. Compared to electric boilers, HPs are praised for their high efficiency, environmental benefits, and advanced intelligence. Based on the reverse Carnot cycle, HPs extract low-grade thermal energy from air, water, or soil, consuming minimal electricity, and then provide usable high-grade thermal energy [45]. Generally, the relationship between the energy input and output of the HP is determined by the Coefficient of Performance (COP).

$$q_{i,t}^{HP} = COP_i^{HP} p_{i,t}^{HP} \quad (17)$$

$$q_{i,\min}^{HP} \leq q_{i,t}^{HP} \leq q_{i,\max}^{HP} \quad (18)$$

where, $q_{i,t}^{HP}$ and $p_{i,t}^{HP}$ are the heat production and electricity consumption of HP i , respectively (kW); $q_{i,\min}^{HP}$ and $q_{i,\max}^{HP}$ define the minimum and maximum thermal power outputs of HP unit i , respectively (kW);

2.4. Storage resources

According to the generalized energy storage framework, the mathematical models of GES and TES typically include four key components: charging/discharging power limits, temporal energy balance based on mass conservation,

capacity limits, and storage restoration. The mathematical model of the GES facility can be expressed as:

$$\begin{cases} 0 \leq g_{i,t}^{\text{GES,c}} \leq g_{i,\max}^{\text{GES,c}}, 0 \leq g_{i,t}^{\text{GES,d}} \leq g_{i,\max}^{\text{GES,d}} \\ SOC_{i,t}^{\text{GES}} = SOC_{i,t-1}^{\text{GES}} + \left(g_{i,t}^{\text{GES,c}} - g_{i,t}^{\text{GES,d}} \right) \Delta t \\ 0 \leq SOC_{i,t}^{\text{GES}} \leq SOC_{i,\max}^{\text{GES}} \\ SOC_{i,t_0}^{\text{GES}} = SOC_{i,t_N}^{\text{GES}} \end{cases} \quad (19)$$

where, $g_{i,t}^{\text{GES,c/d}}$ and $g_{i,\max}^{\text{GES,c/d}}$ are charging/discharging gas flows and its upper limit, respectively (kW); $SOC_{i,t}^{\text{GES}}$ and $SOC_{i,\max}^{\text{GES}}$ are the State of Charge (SOC) of the GES and its maximum storage capacity, respectively (kWh); t_0 and t_N denote the initial and end periods, respectively. Compared to the GES, the mathematical model of the TES facility is slightly adjusted to reflect the significant energy loss during the thermal storage process.

$$\begin{cases} 0 \leq q_{i,t}^{\text{TES,c}} \leq q_{i,\max}^{\text{TES,c}}, 0 \leq q_{i,t}^{\text{TES,d}} \leq q_{i,\max}^{\text{TES,d}} \\ SOC_{i,t}^{\text{TES}} = SOC_{i,t-1}^{\text{TES}} + \left(\eta^{\text{TES,c}} q_{i,t}^{\text{TES,c}} - \frac{q_{i,t}^{\text{TES,d}}}{\eta^{\text{TES,d}}} \right) \Delta t \\ 0 \leq SOC_{i,t}^{\text{TES}} \leq SOC_{i,\max}^{\text{TES}} \\ SOC_{i,t_0}^{\text{TES}} = SOC_{i,t_N}^{\text{TES}} \end{cases} \quad (20)$$

where, $q_{i,t}^{\text{TES,c/d}}$ and $q_{i,\max}^{\text{TES,c/d}}$ are charging/ discharging heat flows and its upper limit, respectively (kW); $\eta^{\text{TES,c/d}}$ is the heat charging/ discharging efficiency; $SOC_{i,t}^{\text{TES}}$ and $SOC_{i,\max}^{\text{TES}}$ are the SOC of the TES and its maximum storage capacity, respectively (kWh); t_0 and t_N denote the initial and end periods, respectively.

3. Energy-carbon pricing-guided collaborative optimization

3.1. Energy-carbon pricing strategy

The key problem for achieving low-carbon and economical operation of the proposed IEC is designing a pricing approach for market participants (producers, prosumers, electrification consumers, and storage resources) to incentivize carbon emission reduction among multiple energy sectors. This study proposes an energy-carbon pricing strategy that establishes mathematical relationships between electricity, gas, and carbon flows by tracking CO₂ production and consumption throughout the local IEC.

The implementation of the proposed strategy follows a two-stage process. First, in the carbon-aware pricing stage, (i) equivalent carbon taxes on electricity and gas are incorporated on the source side, to reflect the environmental costs of carbon emissions from operating-cost functions, and (ii) carbon trading revenues and chemical product sales from P2C processes are accounted for on the load side to count the economic costs of carbon emissions. Then, in the operational optimization stage, the pricing strategy directly links system operation with local market dynamics, enabling price-responsive energy scheduling, flexible resource management, and continuous price-energy feedback.

3.2. Collaborative optimization model

Based on the proposed energy-carbon pricing strategy, this subsection proposes a collaborative optimization model to coordinate multi-vector electrification consumers. This optimization process is structured into two stages: (1) The local market pricing stage incorporates the additional fuel costs associated with a marginal carbon tax on the source side and accounts for the revenue from carbon emission reductions on the load side; (2) the energy management stage focuses on optimizing the real-time operation of each subsystem within the IEC, including energy supply planning, trading volumes, and storage scheduling.

3.2.1. Stage I: local market pricing

Stage I focuses on delivering effective incentive signals among interconnected energy subsystems to ensure that the local IEC achieves both cost-efficient operations and science-based carbon reduction goals. It is assumed that the

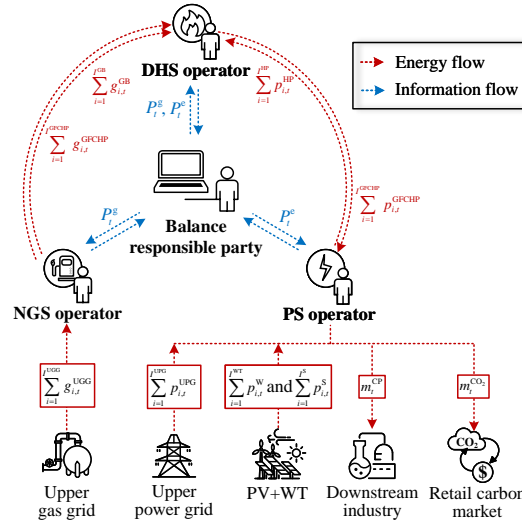


Figure 3: Interactions between subsystem operators and the market manager.

local energy market operates as a perfectly competitive retail market. As illustrated in Fig. 3, each subsystem operator submits the bidding information, including energy purchase and sale volumes to the balance responsible party, while bargaining its required energy transactions with external operators. The social welfare for each subsystem, defined as the net difference between end-user benefits and operating costs, can be calculated as follows [25].

The social welfare for the PS (sw^{PS} , CNY) consists of five components: the revenues from EP selling ECO2R products and trading carbon emission reductions, the revenues from selling electricity to the DHS for operating HPs, the benefits gained by electricity end-users, the expense of purchasing electricity-carbon from the upper power grid, the costs of purchasing electricity generated by GFCHP units from the DHS. Notably, surplus RE electricity within the IEC is completely consumed by the EP and HPs, thus removing the necessity of returning it to the upper grid.

$$sw^{PS} = \sum_{t=1}^T \left[\sum_{j \in J} P^j m_t^{CP} + P^{CET} m_t^{CO_2} + \sum_{i=1}^{I^{HP}} P_t^e p_{i,t}^{HP} + b^{EU} p_t^L - \sum_{i=1}^{I^{UPG}} (P^{UPG} + c^{EECT}) p_{i,t}^{UPG} - \sum_{i=1}^{I^{GFCHP}} P_t^e p_{i,t}^{GFCHP} \right] \quad (21)$$

where, P^j is the market price of ECO2R product j (CNY/kg); P^{CET} is the carbon emission trading price in the local retail carbon market (CNY/kg); P_t^e is the real-time electricity price (kWh); b^{EU} is the utility of electricity end-users (CNY/kWh); P^{UPG} and c^{EECT} are the thermal power price from the upper power grid and the equivalent carbon tax on electricity, respectively (CNY/kWh); I^{HP} , I^{UPG} and I^{GFCHP} denote the number of HPs, nodes connected to the upper power grid, and GFCHP units, respectively.

The social welfare for the NGS (sw^{NGS} , CNY) includes four components: the revenues from selling gas to the DHS for operating GFCHP and GB units, the benefits gained by natural gas end-users, and the expense of purchasing gas-carbon from the upper gas grid.

$$sw^{NGS} = \sum_{t=1}^T \left[\sum_{i=1}^{I^{GFCHP}} P_t^g g_{i,t}^{GFCHP} + \sum_{i=1}^{I^{GB}} P_t^g g_{i,t}^{GB} + b^{GU} g_t^L - \sum_{i=1}^{I^{UGG}} (P^{UGG} + c^{GECT}) \cdot g_{i,t}^{UGG} \right] \quad (22)$$

where, P_t^g is the real-time natural gas price (kWh); b^{GU} is the utility of natural gas end-users (CNY/kWh); g_t^L is the gas load of the NGS (kW); P^{UGG} and c^{GECT} are the gas power price from the upper gas grid and the equivalent carbon tax on natural gas, respectively (CNY/kWh); I^{GB} and I^{UGG} denote the number of GBs and nodes connected to the upper gas grid, respectively.

The social welfare for the DHS (sw^{DHS} , CNY) consists of five components: the revenues from selling electricity generated by the GFCHP unit to the PS, the benefits gained by heat end-users, the costs of purchasing natural gas from the NGS for operating the GFCHP and GB units, and the costs of purchasing electricity from the PS for operating HPs.

$$sw^{\text{DHS}} = \sum_{t=1}^T \left[\sum_{i=1}^{I^{\text{GFCHP}}} P_t^e p_t^{\text{GFCHP}} + b^{\text{HU}} q_t^{\text{D}} - \sum_{i=1}^{I^{\text{GFCHP}}} P_t^g g_{i,t}^{\text{GFCHP}} - \sum_{i=1}^{I^{\text{GB}}} P_t^g g_{i,t}^{\text{GB}} - \sum_{i=1}^{I^{\text{HP}}} P_t^e p_{i,t}^{\text{HP}} \right] \quad (23)$$

where, b^{HU} is the utility of heat end-users (CNY/kWh); q_t^{D} is the actual heat demand of the DHS (kW).

3.2.2. Stage II: energy management

Stage II focuses on energy scheduling formulation within each subsystem to maintain real-time energy balance, minimize network losses, and effectively regulate flexible resources. Assuming that each subsystem operator independently manages its energy system, supervising the entire process of energy production, distribution, conversion, and consumption. The real-time energy balance equations for the PS, NGS, and DHS are expressed as follows:

$$\begin{aligned} \sum_{i=1}^{I^{\text{UPG}}} p_{i,t}^{\text{UPG}} + \sum_{i=1}^{I^{\text{GFCHP}}} p_{i,t}^{\text{GFCHP}} + \sum_{i=1}^{I^{\text{WT}}} p_{i,t}^{\text{W}} + \sum_{i=1}^{I^{\text{PV}}} p_{i,t}^{\text{S}} - \left[\sum_{i=1}^{I^{\text{CS}}} (p_{i,t}^{\text{CS,c}} - p_{i,t}^{\text{CS,d}}) \right] - \left(\sum_{i \in I^{\text{WT}}} p_{i,t}^{\text{WT,S}} + \sum_{i \in I^{\text{PV}}} p_{i,t}^{\text{PV,S}} \right) \\ - \sum_{i=1}^{I^{\text{HP}}} p_{i,t}^{\text{HP}} - p_t^{\text{L}} = \sum_{m=1}^{\Theta^n} p_{mn,t} \end{aligned} \quad (24)$$

$$\sum_{i=1}^{I^{\text{UGG}}} g_{i,t}^{\text{UGG}} - \sum_{i=1}^{I^{\text{GES}}} (g_{i,t}^{\text{GES,c}} - g_{i,t}^{\text{GES,d}}) - \sum_{i=1}^{I^{\text{GFCHP}}} g_{i,t}^{\text{GFCHP}} - \sum_{i=1}^{I^{\text{GB}}} g_{i,t}^{\text{GB}} - g_t^{\text{L}} = \sum_{m=1}^{\Theta^n} g_{mn,t} \quad (25)$$

$$\sum_{i=1}^{I^{\text{GFCHP}}} q_{i,t}^{\text{GFCHP}} + \sum_{i=1}^{I^{\text{GB}}} q_{i,t}^{\text{GB}} + \sum_{i=1}^{I^{\text{HP}}} q_{i,t}^{\text{HP}} - \sum_{i=1}^{I^{\text{TES}}} \left(\eta_{\text{TES,c}} q_{i,t}^{\text{TES,c}} - \frac{q_{i,t}^{\text{TES,d}}}{\eta_{\text{TES,d}}} \right) - q_t^{\text{L}} = \sum_{m=1}^{\Theta^n} q_{mn,t} \quad (26)$$

where, Θ^n defines the set of buses/nodes directly connected to bus/node n ; $p_{mn,t}$, $g_{mn,t}$ and $q_{mn,t}$ are the active power flow through line m - n , the gas flow through pipeline m - n , and the heat flow through pipe m - n , respectively (kW); I^{GES} and I^{TES} denote the number of GES and TES units, respectively.

Heterogeneous energy flows exhibit distinct transmission characteristics across their respective networks, particularly in terms of temporal and spatial scales. Building on previous work in [46], the mathematical models for power and gas flows in the power and natural gas networks can be formulated as follows.

$$\begin{cases} p_{mn,t} = V_{m,t} V_{n,t} (G_{mn} \cos \theta_{mn,t} + B_{mn} \sin \theta_{mn,t}) \\ q_{mn,t}^* = V_{m,t} V_{n,t} (G_{mn} \sin \theta_{mn,t} + B_{mn} \cos \theta_{mn,t}) \end{cases} \quad (27)$$

$$\begin{cases} g_{mn,t} = y_{mn} \sqrt{pr_m^2 - pr_n^2} \\ y_{mn} = y \left(\frac{T^b}{pr^b} \right) d_{mn}^{\frac{5}{2}} \left(\frac{1}{l_{mn} \gamma^G T_{mn}^a \lambda^a f_{mn}} \right) \end{cases} \quad (28)$$

where, $q_{mn,t}^*$ is the reactive power flow through line m - n ; $V_{m/n,t}$, $\theta_{mn,t}$, G_{mn} , and B_{mn} are the bus voltage magnitude, the phase angle difference between buses m and n , and the conductance and susceptance values in the nodal admittances matrix, respectively; pr is the nodal pressure of the pipeline, and y_{mn} is the overall transmission coefficient for pipeline m - n ($\text{m}^3/\text{h} \cdot \text{Pa}$), analogous to the line admittance in the PS. Parameter y_{mn} depends on the physical characteristics of

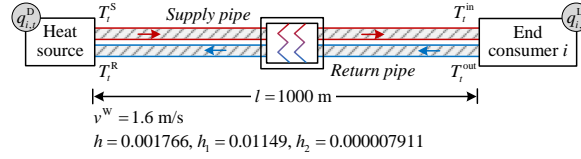


Figure 4: Heat flow in an individual heating pipeline.

pipeline m - n with fixed gas composition. These characteristics include the specific constant γ , base gas pressure pr^b (Pa), base gas temperature T^b (K), pipeline diameter d_{mn} (m), pipeline length l_{mn} (m), specific gravity of natural gas γ^G , average pipeline temperature T_{mn}^a (K), compressibility factor λ^a , and friction factor f_{mn} .

Unlike the instantaneous nature of power flow transmission, heat flow in a network experiences significant time delays. Assuming the DHS within the local IEC operates under a constant-flow variable-temperature control strategy, the dynamic temperature distribution in heating pipelines can be modeled using the function method [47]. Accordingly, the relationship between nodal heat flow, water mass flow, and the inlet and outlet temperatures of each heating pipe is expressed as [48]:

$$\begin{cases} q_{mn,t} = c^W m_{mn} (T_{m,t} - T_{n,t}) \\ T_{n,t} = \varphi_n T_{m,t-\tau_n} + T_i^a (1 - \varphi_n) \end{cases} \quad (29)$$

where, c^W is the specific heat capacity of water (J/kg·K), m_{mn} is the water mass flow (kg/s); $T_{m,t}$, $T_{n,t}$ and T_i^a are the inlet, outlet and ambient temperatures for pipe m - n , respectively (K). Two key parameters τ_n and φ_n represent the delay time (h) and the relative attenuation degree, respectively, characterizing delayed heat transfer and heat loss, as defined in Eq. (30).

$$\begin{cases} \tau_n = \frac{l_n}{v_n^W} \cdot \left[1 + \frac{h_1 h_2}{\omega^2 + (h_1 + h_2)^2} \right] \\ \varphi_n = \exp \left\{ -\frac{h l_n}{v_n^W} \cdot \left[1 - \frac{h_1 (h_1 + h_2)}{\omega^2 + (h_1 + h_2)^2} \right] \right\} \end{cases} \quad (30)$$

where, l_n is the pipe length from the heat source to node n (m); v_n^W is the water velocity at node n (m/s); ω is the angular frequency (rad/s). The physical coefficients of the heating pipe h , h_1 , and h_2 are determined by Eq. (31).

$$h = \frac{k^{WP} L_{mn}^{in}}{A^W c^W \rho^W}, h_1 = \frac{k^{WP} L_{mn}^{in}}{A^P c^P \rho^P}, h_2 = \frac{k L_{mn}^{ex}}{A^P c^P \rho^P} \quad (31)$$

where, k and k^{WP} are the convective heat transfer coefficients between the environment and the pipe outer wall, and between the water flow and the pipe inner wall, respectively (W/m²·K); L_{mn}^{in} and L_{mn}^{ex} are the internal and external perimeters of the pipe wall (m); A^W and A^P are the cross-sectional areas of the water flow and the pipe wall, respectively (m²); c^P is the specific heat capacity of the pipe wall (J/kg·K); ρ^W and ρ^P are the densities of the water and pipe wall, respectively (kg/m³).

Fig. 4 shows an illustrative case for an individual heating pipeline connecting the heat source to end consumer i . The pipeline, comprising a supply pipe and a return pipe, spans 1000 m, with water flow velocity set at 1.6 m/s. Fig. 5 (a) records the indoor temperature T_i^{in} and the ambient temperature T_i^a at the sink node over 24 hours. Fig. 5 (b) shows the supply water temperature T_i^S and the return water temperature T_i^R at the source node, while Fig. 5 (c) presents the actual heat supplied on the source side, calculated using the above heat flow model. The results demonstrate that temporal delays and spatial attenuation in supply and return water temperatures lead to significant discrepancies between the heat supply profile on the source side $p_{i,t}^D$ and the heat load profile on the consumer side $p_{i,t}^L$. As each consumer is located at different distances from the heat source in practice, the DHS operator must consider the load conditions of all consumers to ensure efficient heat source dispatch and maintain real-time supply-demand balance. This emphasizes the necessity of integrating the dynamic heat flow network, with its spatiotemporal characteristics, into the IEC system.

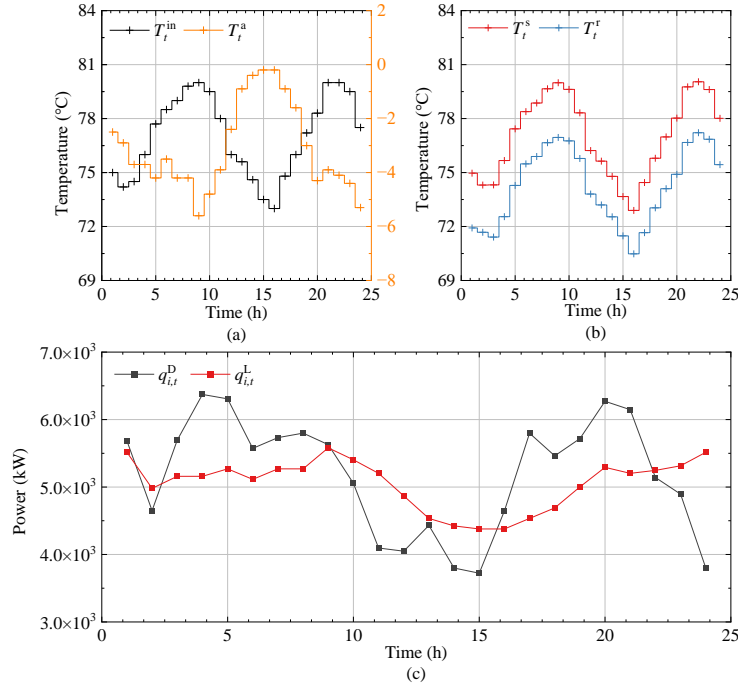


Figure 5: Temperature distribution and heat supply, (a) indoor and ambient temperature, (b) supply and return water temperature, and (c) actual heat supplied on the source side.

3.2.3. Model formulation

In the local IEC, each subsystem operator develops an hourly energy scheduling plan for internal equipment while engaging in external interactions to pursue its respective interests in the market. The collaborative optimization objective for each subsystem to maximize social welfare is formulated as follows.

$$\max F = \left\{ \max_{\mathbf{x}^{PS}, P_t^e} sw^{PS}, \max_{\mathbf{x}^{NGS}, P_t^g} sw^{NGS}, \max_{\mathbf{x}^{DHS}, P_t^e, P_t^g} sw^{DHS} \right\} \quad (32)$$

where, \mathbf{x}^{PS} , \mathbf{x}^{NGS} , and \mathbf{x}^{DHS} define the sets of decision variables associated with the operations of the EP (as defined in Eq. (21)), NGS (as defined in Eq. (22)), and DHS (as defined in Eq. (23)), respectively.

Besides the equipment operation models, energy balance equations, and energy flow models discussed earlier, each subsystem is subject to the constraints of its respective network transmission capacity.

$$|p_{mn,t}| \leq p_{mn,max} \quad (33)$$

$$|g_{mn,t}| \leq g_{mn,max} \quad (34)$$

$$|q_{mn,t}| \leq q_{mn,max} \quad (35)$$

where, $p_{mn,max}$, $g_{mn,max}$ and $q_{mn,max}$ are transmission limit of power line $m - n$, gas pipeline $m - n$, and heating pipe $m - n$, respectively (kW).

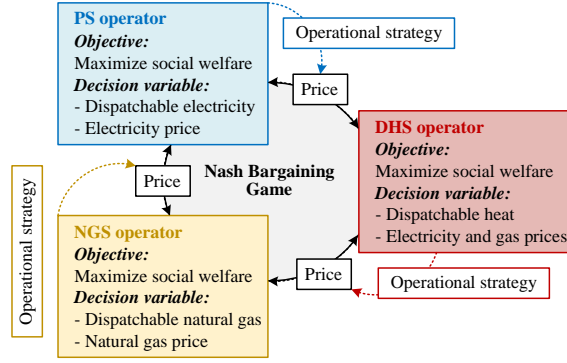


Figure 6: Schematic diagram of Nash bargaining game.

Therefore, the collaborative optimization model can be summarized as follows.

$$\begin{aligned}
 &\hookrightarrow \max_{\mathbf{x}^{\text{PS}}, P_t^e} sw^{\text{PS}} \\
 &s.t. \mathbf{x}^{\text{PS}} \text{ subject to formula:} \\
 &\quad (1) - (3), (9) - (16), (24), (27), (33) \\
 &\hookrightarrow \max_{\mathbf{x}^{\text{PS}}, P_t^e, P_t^g} sw^{\text{NGS}} \\
 &s.t. \mathbf{x}^{\text{NGS}} \text{ subject to formula:} \\
 &\quad (19), (25), (28), (34) \\
 &\hookrightarrow \max_{\mathbf{x}^{\text{PS}}, P_t^e, P_t^g} sw^{\text{DHS}} \\
 &s.t. \mathbf{x}^{\text{DHS}} \text{ subject to formula:} \\
 &\quad (4) - (8), (17), (18), (20), (26), (29) - (31), (35)
 \end{aligned} \tag{36}$$

3.3. Nash bargaining game framework

In most research assumptions, a centralized dispatching entity oversees the operation, coordination, and management of local IECs, ensuring flexible and reliable energy services across subsystems while maximizing overall benefits. However, Chinese energy sectors present unique challenges, including information asymmetry, substantial communication costs, and legitimate concerns over commercial confidentiality among different energy operators. These constraints often lead to incomplete information sharing, as local subsystem operators tend to protect their individual interests during decision-making processes.

This study employs a Nash bargaining game framework [27], which is particularly suitable for modeling such decentralized decision-making scenarios in energy systems. The Nash bargaining game-theoretic approach provides a solution that balances the interests of multiple stakeholders (PS, NGS, and DHS operators) while considering their individual rationality constraints. The game framework enables Pareto-optimal solutions that ensure: (i) individual rationality, where each market participant's benefit is at least as good as their non-cooperative outcome, (ii) collective efficiency, maximizing the joint benefits of all participants, and (iii) fairness in benefit distribution, effectively resolving conflicts of interest among subsystem operators while maintaining operational privacy, as only limited information exchange is required through the negotiation process.

3.3.1. Game process

The Nash bargaining game framework for the proposed collaborative optimization model is illustrated in Fig. 6. Each subsystem operator consolidates bidding information from its managed producers, prosumers, consumers, and storage resources to engage in energy trading within the local energy market, aiming to maximize its social welfare. Accordingly, the Nash bargaining game model is formulated as follows [49].

$$G^{NB} = \left\{ N^P, \{S_i\}_{i=1}^{N^P}, \{B_i\}_{i=1}^{N^P} \right\},$$

$$\begin{cases} N^P = \{ \text{PS, NGS, and DHS operators} \} \\ \{S_i\}_{i=1}^{N^P} = \{ \{ \mathbf{x}^{\text{PS}}, \mathbf{x}^{\text{NGS}}, \mathbf{x}^{\text{DHS}} \}, \{ P_t^e, P_t^g \} \} \\ \{B_i\}_{i=1}^{N^P} = \{ sw^{\text{PS}}, sw^{\text{NGS}}, sw^{\text{DHS}} \} \end{cases} \quad (37)$$

This game model contains three elements: participants N^P , their strategy sets S_i , and the corresponding benefits B_i . These elements are described as follows.

- (1) Participants: The PS, NGS and DHS operators participate in the local retail market process as unified representatives of their respective market roles.
- (2) Strategy set: The energy-carbon pricing strategy for the external market game adjusts the real-time gas and electricity prices, expressed as P_t^e, P_t^g , while the energy management strategy for the internal operation optimizes the energy schedules, expressed as $\mathbf{x}^{\text{PS}}, \mathbf{x}^{\text{NGS}}, \mathbf{x}^{\text{DHS}}$.
- (3) Benefits: The benefits for each participant correspond to their social welfare defined in the objective function, expressed as $sw^{\text{PS}}, sw^{\text{NGS}},$ and sw^{DHS} .

3.3.2. Nash equilibrium

The iterative game process among stakeholders progresses until an equilibrium is reached. Throughout this process, all operators hold equal market positions, making independent and self-interested decisions simultaneously. When other subsystems have determined their strategies, a given subsystem adjusts its strategy to maximize its benefits among the available options, known as the optimal response. A stable equilibrium is achieved when a strategy solution satisfies the optimal response for all subsystems while ensuring that no operator can unilaterally adjust its strategy to gain additional benefits [50]. This equilibrium condition is expressed as follows.

$$s_i^* = \arg \max_{s_i \in S_i} B_i(s_i, s_{-i}^*) \quad (38)$$

where s_i^* is the optimal strategy of subsystem i and s_{-i}^* is optimal strategies of all other subsystems except i .

3.3.3. Solution method

Based on Brouwer's fixed-point theorem [51], a Nash equilibrium exists if the proposed model satisfies the nonempty, convex, and compact properties. Current mainstream approaches to solving Nash bargaining optimization problems are categorized into two methods: (1) Karush-Kuhn-Tucker (KKT) transformation method leverages the KKT conditions to convert the primal problem into a dual problem formulation for an easier solution; (2) distributed Iterative solution uses analytical methods or metaheuristic algorithms to solve the multi-stage/level/objective optimization problems[52], [53]. Given that the non-convex gas network constraints in Eq. (28) can be reconstructed into a convex form, as detailed in our previous work [54], this study adopts the KKT transformation method for its computational efficiency. The reformulated Nash bargaining game model, incorporating the KKT conditions, is expressed as follows.

$$s_i = \arg \min_{s_i \in S_i} -B_i(s_i, s_{-i})$$

$$s.t. \begin{cases} h(s_i, s_{-i}) = 0 \\ g(s_i, s_{-i}) \leq 0 \end{cases}$$

$$\rightarrow \begin{cases} L_i(s_i, s_{-i}, \lambda_i, \mu_i) = -B_i(s_i, s_{-i}) + \sum \lambda_i h(s_i, s_{-i}) + \sum \mu_i g(s_i, s_{-i}) = 0 \\ \frac{\partial L_i(s_i, s_{-i}, \lambda_i, \mu_i)}{\partial s_i} = 0 \\ \mu_i = 0 \\ h(s_i, s_{-i}) = 0 \\ g(s_i, s_{-i}) \leq 0 \end{cases} \quad (39)$$

where, L_i is the Lagrangian function; λ_i and μ_i are the Lagrange multipliers associated with equality and inequality constraints, respectively, also known as dual variables.

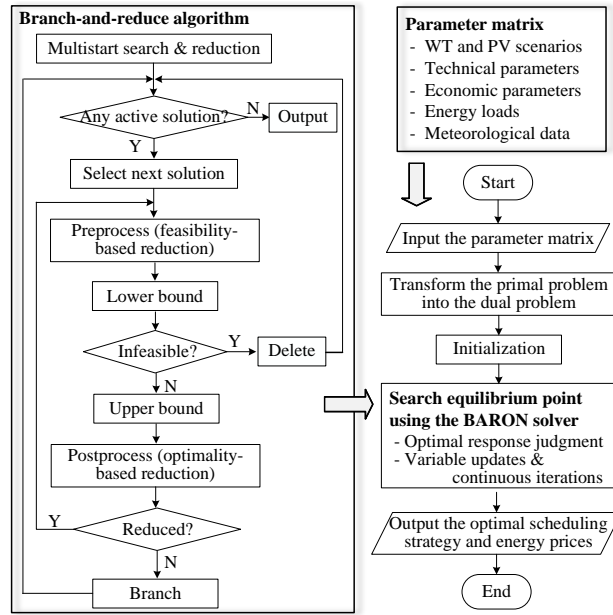


Figure 7: Flow chart of the solution process.

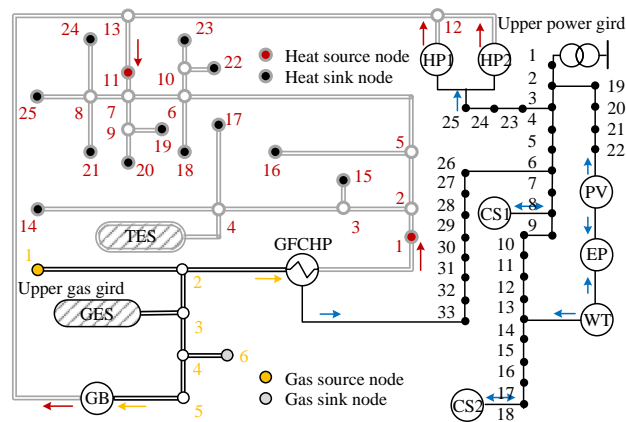


Figure 8: Topology of the test system.

Using time t as the index, the optimization model in Eq. (39) comprises: (1) 64 sets of decision variables, including dual variables, operating variables, and price variables; (2) 72 sets of scalar parameters; (3) 96 groups of equality and inequality constraints. The specific solution flowchart is shown in Fig. 7. This work uses the BARON solver on GAMS 47.2.0 to solve the proposed optimization problem. The BARON solver, built on the branch-and-reduce algorithm, handles most current mainstream optimization problems, including linear programming, non-linear programming, mixed-integer programming, and mixed-integer nonlinear programming.

4. Case study

The effectiveness of the proposed approach is validated in an IEC that includes a modified IEEE 33-bus PS, a 6-node NGS, and a 25-node DHS, as illustrated in Fig. 8. Simulations are conducted on a laptop with an Intel Core i7-12700H CPU and 16 GB RAM.

Table 3
Economic parameters of the test system.

Symbol	Value	Symbol	Value
P^{UPG}	0.6 CNY/kWh	P^{CO}	1.4 CNY/kg
c^{PEN}	0.2 CNY/kWh	$P^{Ethylene}$	7.5 CNY/kg
P^{UGG}	0.45 CNY/kWh	$P^{Formicacid}$	3.4 CNY/kg
c^{CT}	0.05 CNY/kg	$P^{Ethanol}$	5.6 CNY/kg
c^{GECT}	0.0165 CNY/kWh	$P^{Methanol}$	2.8 CNY/kg
c^{EECT}	0.0499 CNY/kWh	P^{H_2}	30 CNY/kg
P^{CET}	0.035 CNY/kg	c^{H_2TR}	7.0 CNY/kWh
α^{EP}	0.2	b^{EU}	0.5 CNY/kWh
b^{GU}	0.35 CNY/kWh	b^{HU}	0.2 CNY/kWh

Table 4
Technical parameters of the test system.

Unit	Capacity	Power limit	Efficiency	Climbing limit
Upper gas grid	350 MWh	0-350 MWg	-	210 MWg
Upper power grid	250 MWh	0-250 MWe	-	150 MWe
GFCHP	100 MWh	15-100 MWe	0.9	60 MWe
EP	150 MWh	0-150 MWe	-	90 MWe
WT	250 MWh	0-250 MWe	-	-
PV	75 MWh	0-75 MWe	-	-
GB	60 MWh	6-60 MWt	0.95	-
HP1	45 MWh	0-45 MWt	3	-
HP2	45 MWh	0-45 MWt	3	-
CS1	60 MWh	0-60 MWe	0.85	-
CS2	60 MWh	0-60 MWe	0.85	-
GES	20 MWh	0-5 MWg	1	-
TES	20 MWh	0-5 MWt	0.95	-

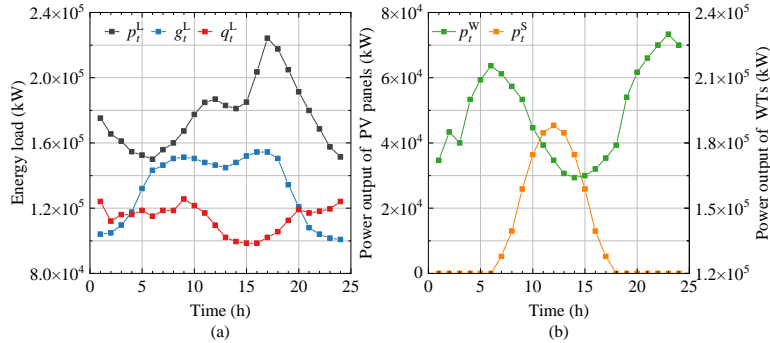


Figure 9: Profiles of (a) energy loads and (b) PV and WT power outputs.

4.1. System parameters

The modified IEEE 33-bus PS operates a group of WTs, PV panels, two CSs, an EP, and the electricity use of the upper power grid. The 6-node NGS controls a GES facility and gas use of the upper gas grid. The 25-node DHS manages a GFCHP unit, a GB, two HPs, and a TES facility. The scheduling period is set to 24 hours with a time scale of 1 hour. Detailed economic and technical parameters are provided in Tables 3 and 4. In the DHS, each sink node acts as an exchange station supplying heat to local end users. Parameters related heating network are given in Table 5, where $K = ^\circ\text{C} + 273$. Additionally, the day-ahead profiles for electricity, gas, and heat loads are shown in Fig. 9 (a), while the PV and WT power outputs for a typical winter day are illustrated in Fig. 9 (b).

Table 5
Heating network parameters.

Node	Source type	L_{mn}^{in} (m)	L_{mn}^{ex} (m)	l_n (m)	v_n^{W} (m/s)
14	CHP	1.884	2.041	3560	0.8
15	CHP	1.884	2.041	990	0.8
16	CHP	1.884	2.041	2010	0.8
17	CHP	1.884	2.041	2760	0.8
18	GB&HP	0.942	1.0205	1000	1.6
19	GB&HP	0.942	1.0205	800	1.6
20	GB&HP	0.942	1.0205	800	1.6
21	GB&HP	0.942	1.0205	500	1.6
22	GB&HP	0.942	1.0205	1000	1.6
23	GB&HP	0.942	1.0205	1000	1.6
24	GB&HP	0.942	1.0205	500	1.6
25	GB&HP	0.942	1.0205	500	1.6
Parameter	Value	Parameter	Value	Parameter	Value
c^{W}	4200 J/kg·K	ρ^{W}	971.8 kg/m ³	k^{WP}	1131.11 W/m ² ·K
c^{P}	460 J/kg·K	ρ^{P}	7850 kg/m ³	k	0.6867 W/m ² ·K

Table 6
Different compositions of electrification consumers.

Case	P2C	EV	P2H	Description
1	√	√	√	Proposed IEC
2	√	×	√	IEC without CSs
3	×	√	√	IEC without EP
4	×	×	√	IEC without EP and CSs
5	√	√	×	IEC without HPs
6	×	×	×	Conventional community

4.2. Case settings

This study designs and simulates several cases to reflect different compositions of electrification consumers, aiming to evaluate the performance advantages of the constructed IEC and the application value of the proposed optimization approach. The discussions and analyses of numerical results are centered on four key perspectives: pricing outcomes, performance improvements, electricity demand reshaping, and flexibility services. The test system is simulated in six cases, as summarized in Table 6.

To ensure the simulation proceeds smoothly, the following assumptions are emphasized:

- (1) Each energy unit is dispatched by the corresponding energy subsystem it serves. For instance, the GB is operated by the DHS to provide heat service, while the GFCHP unit is specified to be dispatched by the DHS operator based on the principle of determining power based on heat.
- (2) The main product of the EP is set as ethanol, with other chemical by-products generated at a uniform conversion efficiency.
- (3) The test system prioritizes the use of PV power, followed by wind power, and local RE electricity is free.
- (4) The DHS within the IEC adopts a constant-flow variable-temperature control strategy, while the variation of the gas content in a pipeline is restricted within a narrow limit.
- (5) In cases with P2C consumers, surplus RE electricity is fully utilized by the EP. In contrast, without P2C consumers, excess RE electricity is directly curtailed incurring a penalty cost of 0.2 CNY/kWh.

4.3. Results, discussion, and analysis

In this section, representative results from the six cases are compared and analyzed in the following subsections to comprehensively evaluate the potential benefits of the proposed IEC and its optimization approach.

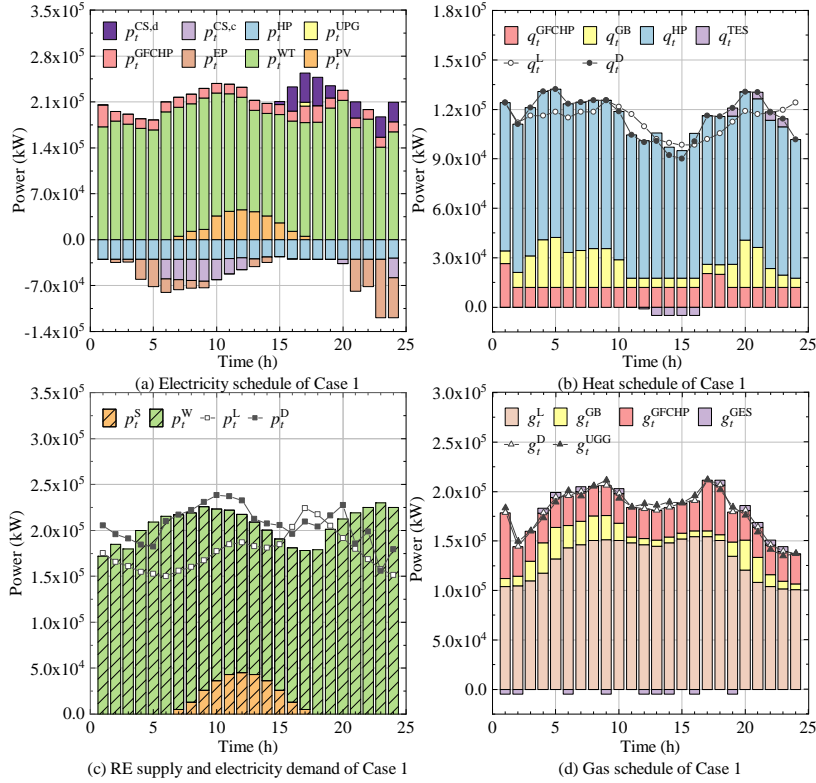


Figure 10: Energy scheduling results for Case 1

4.3.1. Energy scheduling

As shown in Fig. 9, a typical mismatch between power load and wind power output results in RE curtailments during low-demand periods and electricity shortages during peak-demand periods. Fig. 10 illustrates the energy scheduling results of the proposed IEC (Case 1).

Fig. 10 (a) shows the optimal electricity scheduling strategy for the IEC (Case 1). During peak-demand periods, the PS operator issues scheduling commands instructing EV owners to adjust their original charging plans. In response, EV owners shift their charging times from 15:00–19:00, 21:00, and 23:00–24:00 to 6:00–12:00, 20:00, and 24:00. During low-demand periods, the EP utilizes surplus RE electricity and CO₂ captured for chemical production. Additionally, since the power consumption of HPs is directly influenced by the heat demand, the complementary characteristics of electricity and heat loads positively impact actual electricity demand. As shown in Fig. 10 (c), the proposed optimization strategy effectively mitigates the imbalance between power demand and RE supply by coordinating the operation of three electrification consumers: EVs, P2C, and P2H. This coordination reduces the local IEC's reliance on the upper power grid ($p_t^{\text{UPG}} = 0$) while fully meeting users' electricity demands.

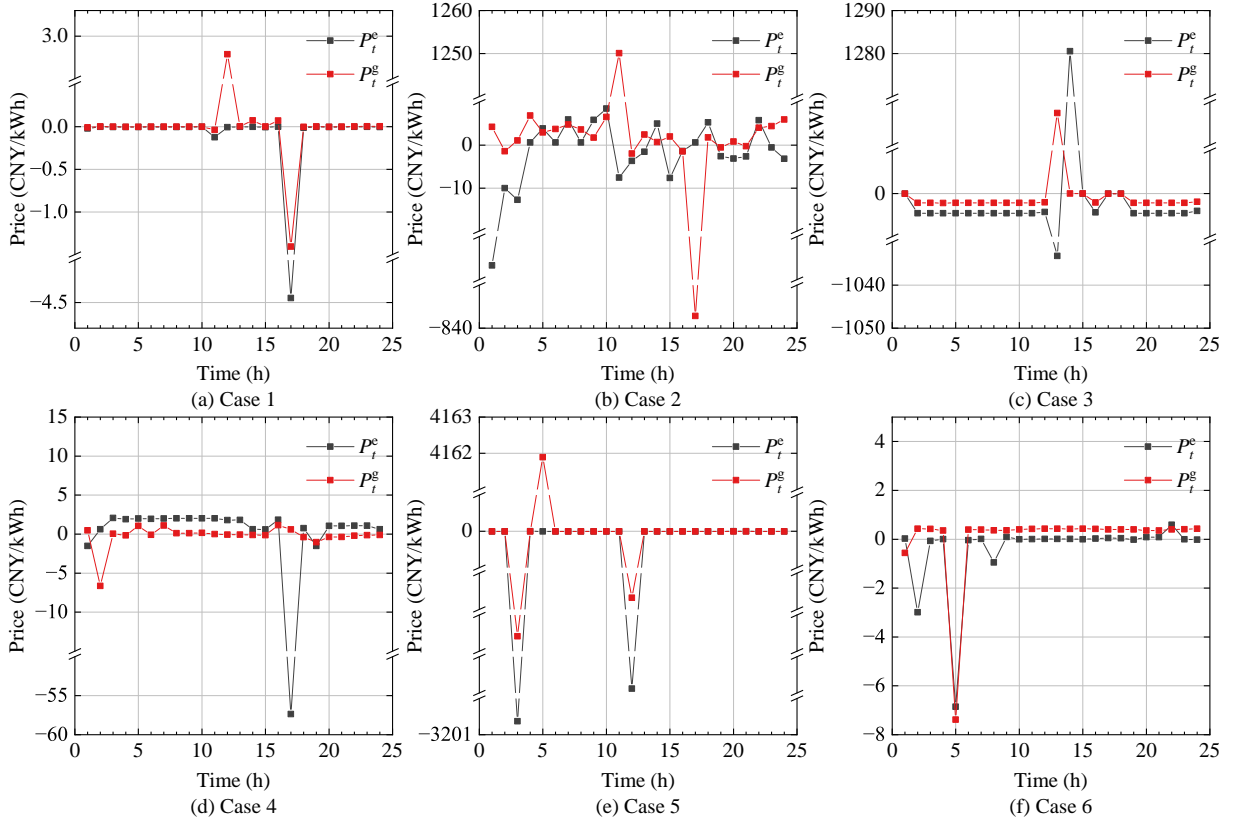
Figs. 10 (b) and (d) illustrate optimal heat and gas scheduling strategies for the IEC, respectively. Due to superior heat conversion efficiency, the DHS operator prefers using HP for heating over DHS and GB. Notably, in Fig. 10 (b), a clear spatiotemporal difference exists between the actual heat production on the source side and the reported heat load from end users. This difference is attributed to both time delays and heat losses at sink nodes 14–25, as derived in Eq. (30). The calculated time delays and relative attenuation degrees for nodal temperatures are presented in Table 7. Furthermore, TES and GES facilities provide flexibility to the DHS and NGS, respectively, although their adjustment capabilities are limited by their individual storage capacities.

The optimal scheduling results of Case 1 preliminarily demonstrate the effectiveness of the proposed IEC framework and optimization approach. The energy scheduling results for Cases 2–6 are presented in Fig. A1 in the appendix.

Table 7

Calculated time delays and relative attenuation degrees for nodal temperatures.

Node	14	15	16	17	18	19	20	21	22	23	24	25
τ_n	1.236	0.172	0.698	0.958	0.174	0.139	0.139	0.087	0.174	0.174	0.087	0.087
φ_n	0.9981	0.9997	0.9988	0.9984	0.9997	0.9997	0.9997	0.9998	0.9997	0.9997	0.9998	0.9998

**Figure 11:** Energy-carbon integrated pricing results for six cases.

In Cases 1–4, which incorporate P2H, as illustrated in Fig. 10 (a) and Figs. A1 (a), (d), and (g), only the PS with EVs can fully meet the electricity demand without relying on the upper power grid. In contrast, in Cases 5 and 6, which lack P2H, as shown in Figs. A1 (k) and (n), the DHS operator prefers to increase the CHP output to satisfy the heat demand. However, as shown in Figs. A1 (j) and (m), increasing the CHP output also leads to a significant surplus of RE electricity ($p_t^{\text{RE,spill}}$). In Case 5, the PS operator can utilize the EP to absorb this surplus RE electricity. Conversely, in Case 6, which lacks electrification consumers, the surplus RE electricity must be curtailed, incurring penalty costs.

4.3.2. Pricing outcomes

The numerical results of real-time electricity and gas prices for the six cases are illustrated in Fig. 11. Since local RE electricity is assumed to be free in this study, when energy prices are entirely determined by the local retail energy market, an oversupply condition may lead subsystem operators to sell energy at zero or even negative prices during certain periods to avoid energy wastage.

Table 8 summarizes fluctuation ranges (peak and valley values) of electricity and gas prices across the six cases. In Case 1, which includes all types of electrification consumers, energy price profiles are relatively stable. In Case 2, which excludes EV consumers, energy price fluctuations are significant. For instance, gas prices reach a peak of 1250.09 CNY/kWh and a valley of -837.17 CNY/kWh. In Case 3, which excludes P2C consumers, energy prices drop into negative values for most periods due to the reduced competition between the EP and end users for RE

Table 8
Fluctuation ranges of electricity and gas prices.

Case	P_t^e band	P_t^g band
1	[-4.75, -0.00026]	[-1.11, 0.59]
2	[-56.72, 8.47]	[-837.17, 1250.09]
3	[-1033.21, 1280.52]	[-2.17, 107.43]
4	[-57.36, 2.069]	[-6.63, 1.15]
5	[-3200.63, -0.000072]	[-3040.59, 4161.89]
6	[-6.86, 0.59]	[-7.38, 0.43]

Table 9
Economic and environmental benefits for the six cases.

Case	Operating cost	CO ₂ reduction	Surplus RE
1	1,955,410 CNY	106,762 kg	396,740 kWh
2	2,016,950 CNY	146,248 kg	543,478 kWh
3	2,103,660 CNY	0 kg	396,287 kWh
4	2,220,110 CNY	0 kg	543,315 kWh
5	2,811,710 CNY	226,825 kg	842,911 kWh
6	3,202,530 CNY	0 kg	947,637 kWh

electricity. However, extreme energy prices persist, such as a peak electricity price of 1280.52 CNY/kWh at 14:00, a valley electricity price of -1033.21 CNY/kWh at 13:00, and a peak gas price of 107.43 CNY/kWh at 13:00. Case 4, excluding both EV and P2C consumers, shows increased electricity prices, with a valley price of -57.36 CNY/kWh at 17:00. In Case 5, which excludes P2H consumers, energy prices extremely worsen, with peak-to-valley differences of 7202.48 CNY/kWh for gas and 3200.63 CNY/kWh for electricity. Finally, in Case 6, which adopts the conventional cogeneration operation mode, energy prices are primarily influenced by marginal costs of thermal power, RE electricity, and natural gas from the upper gas grid. The valley prices for electricity and gas occur at 5:00, reaching -6.86 CNY/kWh and -7.38 CNY/kWh, respectively.

The observed price variations across the six cases highlight the impact of different electrification consumer compositions on energy price profiles within the IEC. The results demonstrate that collaboration among EV, P2C, and P2H consumers effectively absorbs surplus RE, balances energy supply and demand, and stabilizes natural gas and electricity price fluctuations.

4.3.3. Performance improvements

Table 9 shows the superior performance of the proposed IEC in reducing operating costs, reducing carbon emissions, and enhancing local RE integration. Compared to the conventional CHP community system, the proposed IEC achieves daily operating cost savings of 1,247,120 CNY and CO₂ reduction of 106,762 kg. In the cases that include P2C consumers (Cases 1, 2, and 5), surplus RE electricity is fully utilized by the EP for chemical production. Thus, Case 1 reduces actual RE curtailment by 947.637 kWh compared to Case 6.

Despite increased utilization of excess RE electricity for chemical production in Cases 2 and 5, Case 1 demonstrates the best economic benefit, namely achieving the lowest operating cost of 1,955,410 CNY, attributed to the flexible coordination of multi-vector electrification consumers. Extrapolating these results over the typical five-month heating season in Chinese cities, the proposed IEC could annually save approximately 190 million CNY in operating costs and reduce carbon emissions by 16,014 tons.

4.3.4. Electricity demand reshaping

Fig. 12 illustrates the actual electricity demand profiles for IEC operations across the six cases. Initially, the power load curve mismatches with the local RE power generation curve, such as during 16:00–19:00, where RE generation valleys while electricity demand peaks.

As shown in Fig. 12 (a), the proposed IEC effectively reshapes electricity demand during the scheduling period. Comparisons among Case 2 (Fig. 12 (b)), Case 3 (Fig. 12 (c)), and Case 5 (Fig. 12 (e)), where EV, P2C, and P2H consumers are excluded, respectively, show that EVs have the most significant impact on improving electricity demand. In Case 4 (Fig. 12 (d)) the role of P2H in demand reshaping is minimal when diverse heating options and sufficient heat

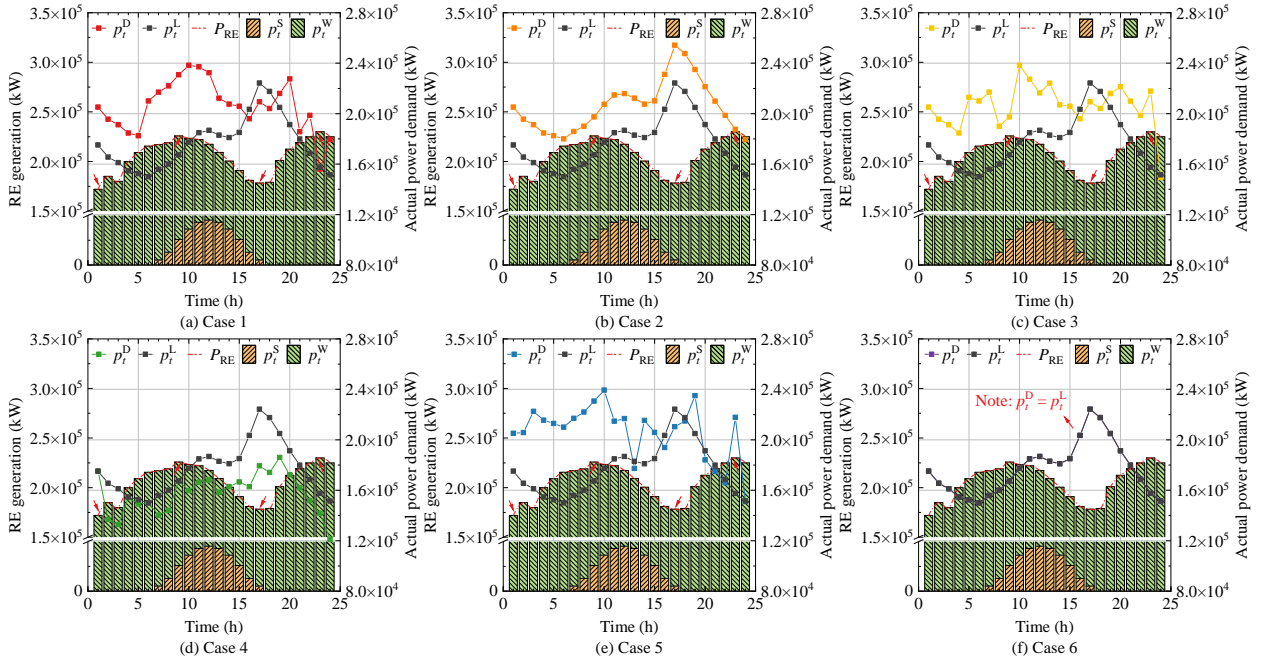


Figure 12: Electricity demand reshaping for six cases.

sources are available. Although P2C is less effective than EVs in reshaping electricity demand, a comparison between Case 1 (Fig. 12 (a)) with Case 3 (Fig. 12 (c)) shows that P2C consumers contribute to a smoother electricity demand profile.

These simulation results confirm that the proposed IEC effectively reshapes electricity demand through coordinated dispatch of multi-vector electrification consumers, ensuring better tracking of local RE generation. EVs demonstrate exceptional load-shaping capabilities, while P2C consumers help reduce load fluctuations.

4.3.5. Flexibility services

Fig. 13 presents the operational statuses of TES and GES facilities across the six cases. In Case 1, as shown in Figs. 10, 11 (a), and 13 (a), TES and GES units store energy during valley demand and low prices and release energy during peak demand and high prices, enhancing their respective subsystem flexibility and improving the IEC's economic performance. In Cases 1–4, which include P2H consumers, TES activities are concentrated between 10:00 and 23:00, allowing the DHS to fully utilize surplus RE electricity by adjusting the heat demand. Even in Cases 5 and 6, without P2H consumers, the TES continues to provide flexibility, as the CHP unit bridges energy interaction between the PS and the DHS. On the other hand, GES activities decline in Cases 2, 4, and 6, which exclude EVs. Combining Fig. 12 and Fig. 13, it is evident that GES charging and discharging activities are closely related to variations in reshaped electricity demand. These findings confirm the contribution of TES and GES facilities in delivering shared flexibility services to the PS through network interconnection within the IEC.

To analyze the impact of multi-vector electrification consumers on IEC performance, this study examines γ and COP_i^{HP} as control variables representing the flexibility levels of EV and P2H consumers. Figs. 14 and 15 illustrate IEC performance under varying flexibility levels of these consumers. In scenarios where COP_i^{HP} is fixed at 3, an increase in dispatchable EVs enhances social welfare and reduces surplus RE electricity. However, greater EV participation increases its RE electricity consumption, limiting the RE electricity available for EP operations and reducing both electrochemical benefits and CO_2 emission reductions.

In scenarios with γ set to 20%, increasing the HP's COP initially improves social welfare and reduces surplus RE electricity. Higher COP levels encourage DHS operators to prioritize HPs for heating, boosting RE electricity utilization. Once COP exceeds a certain threshold, the electricity required for the same amount of heat decreases,

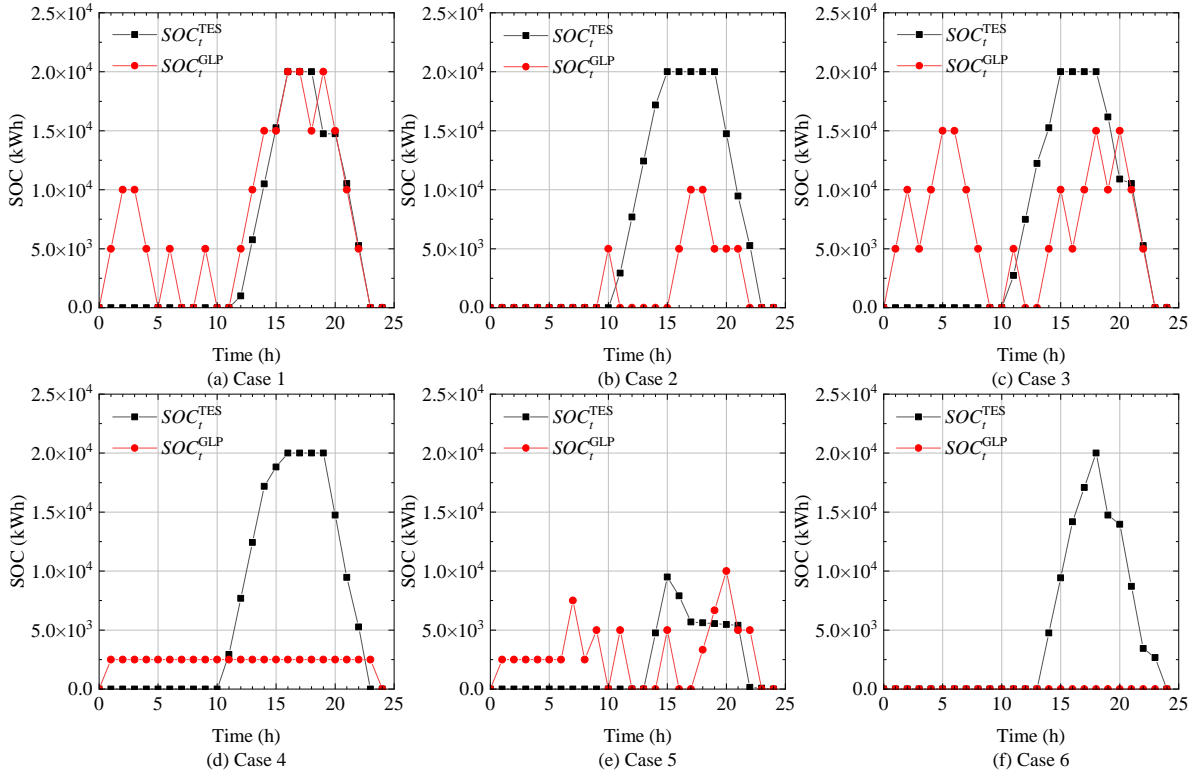


Figure 13: Operational statuses of TES and GES facilities for six cases.

leaving more RE electricity available for EP operations, thus increasing electrochemical benefits and further reducing CO₂ emissions.

5. Conclusion

This paper proposes a novel energy-carbon pricing-guided collaborative optimization model for a local IEC that achieves both cost-effective energy supply and market-competitive carbon emission reduction. The model integrates multi-vector electrification consumers to align with local RE generation while efficiently utilizing carbon-emitting sources. This approach offers opportunities for the IEC to participate in carbon emission trading and generate revenue through electrochemical product sales. Using a Nash bargaining game framework, the proposed optimization strategy balances economic and environmental benefits, enhancing coordination among cross-sector storage resources and electrification consumers. Case studies involving six scenarios of electrification consumer compositions validate the model's effectiveness, leading to the following conclusions:

- (1) The collaboration among EV, P2C, and P2H consumers effectively absorbs surplus RE, balances energy supply and demand, and mitigates price fluctuations.
- (2) While EVs and P2H consumers compete with P2C for RE electricity, reducing electrochemical revenues, the proposed IEC still achieves the lowest daily operating cost of 1,247,120 CNY and a CO₂ reduction of 106,762 kg.
- (3) The proposed model effectively reshapes initial electricity demand during the scheduling period, with EVs having the most significant impact on demand improvement and P2C consumers contributing to smoother demand profiles.
- (4) TES and GES share their flexibility with the PS through network interconnection within the IEC. Higher flexibility levels of EV and P2H consumers lead to the higher social welfare of the IEC, however, negatively impact P2C operations, thereby limiting CO₂ emission reductions.

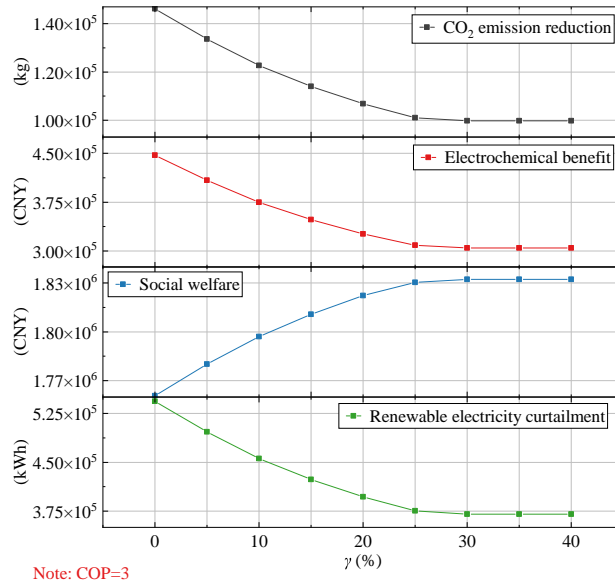


Figure 14: Performance on varying flexibility levels of EVs.

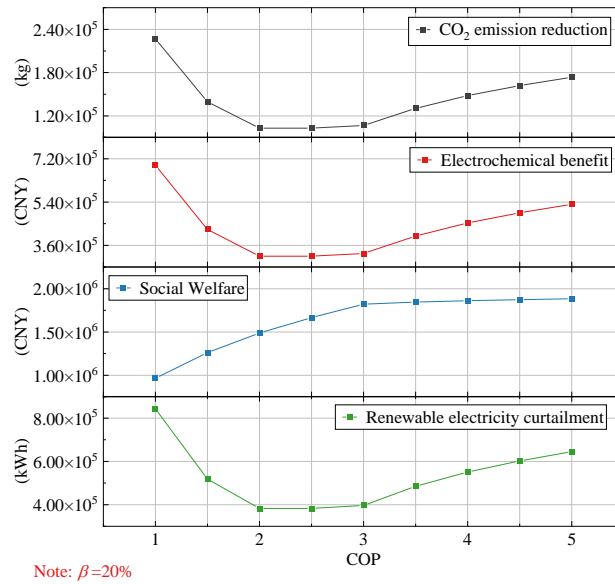


Figure 15: Performance on varying flexibility levels of P2H.

The reliance of this study on a 24-hour scheduling period may constrain the ability to comprehensively evaluate the long-term performance impacts of the IEC. Additionally, in practical ECO2R reactions, even high-performance catalysts cannot guarantee precise control over specific product yields. Future research will address these uncertainties, as well as the variability in renewable energy, to improve the model's accuracy and robustness.

Acknowledgment

This work was funded in part by the Innovation Support Program (Soft Science Research) of Jiangsu Province of China [BE2023093-1] and in part by UK Research and Innovation (UKRI) under the UKRI Postdoctoral Fellowship Guarantee Grant [EP/Z001889/1]. The authors would like to acknowledge the Department of Engineering, University of Cambridge, for the support of the Fellowship. The contents reflect only the authors' view and not the views of the University or the UKRI.

Appendix

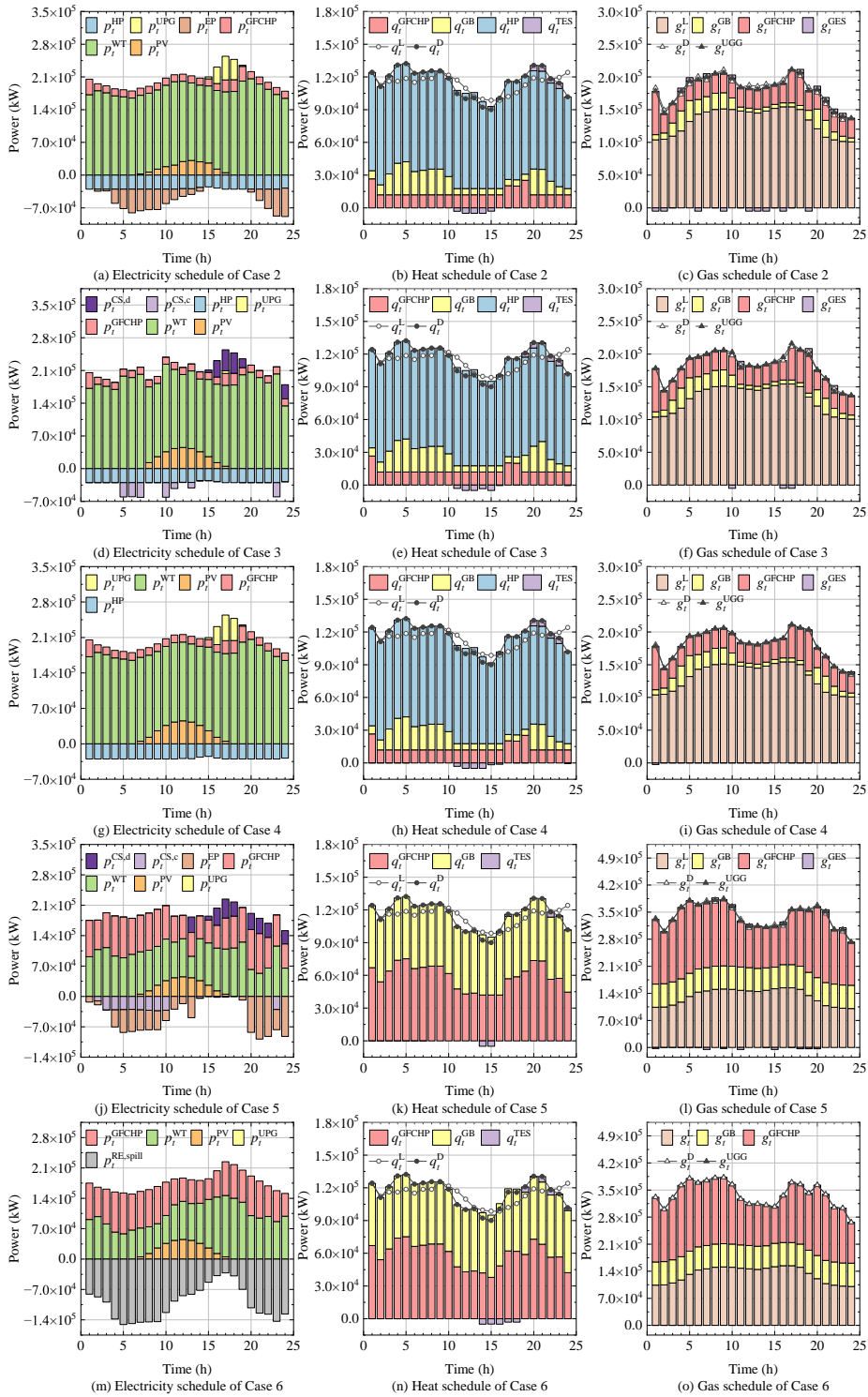


Figure A1: Energy scheduling results for Cases 2-6

References

- [1] N. Yan, G. Ma, X. Li, J. M. M. Guerrero, Low-carbon economic dispatch method for integrated energy system considering seasonal carbon flow dynamic balance, *IEEE Trans. Sustainable Energy* 14 (1) (2023) 576–586.
- [2] W.-M. Małgorzata, F. Nicolas, J. Dave, A. Katye, B. Richard, B. Hannah, B.-L. Chelsea, E. Matt, M. Phil, R. Kostantsa, B. Sarah, C. Libby, D. Reynaldo, H. Rosamond, H. Sam, H. Leo, H. Sanghyun, L. Uni, L. Aditya, M. Josie, R. James, R. Neshwin, R. Chris, Z. Oya, *Global electricity review 2024*, Tech. rep., Ember (2024).
- [3] M. R. Abdussami, A. Verma, Future energy landscapes: Analyzing the cost-effectiveness of nuclear-renewable integrated energy systems in retrofitting of coal power plants, *Appl. Energy* 377 (1) (2025) 1–18.
- [4] X. Zhang, L. Che, M. Shahidehpour, A. Alabdulwahab, A. Abusorrah, Electricity-natural gas operation planning with hourly demand response for deployment of flexible ramp, *IEEE Trans. Sustainable Energy* 7 (3) (2016) 996–1004.
- [5] N. Lou, Y. Zhang, Y. Wang, Q. Liu, H. Li, Y. Sun, Z. Guo, Two-stage congestion management considering virtual power plant with cascade hydro-photovoltaic-pumped storage hybrid generation, *IEEE Access* 8 (2020) 186335–186347.
- [6] L. Sun, Y. Li, L. Li, J. Yu, L. Li, C. Xu, Operation flexibility analysis of combined heat and power plant using high and low bypass, in: *2024 6th Asia Energy and Electrical Engineering Symposium (AEEES)*, 2024.
- [7] G. Abbas, Z. Wu, A. Ali, Multi-objective multi-period optimal site and size of distributed generation along with network reconfiguration, *IET Renew. Power Gener.* 18 (16) (2024) 3704–3730.
- [8] V. Kleinschmidt, T. Hamacher, V. Peric, M. R. Hesamzadeh, Unlocking flexibility in multi-energy systems: a literature review, in: *2020 17th International Conference on the European Energy Market (EEM)*, 2020.
- [9] Y. Xi, Z. Zhang, J. Zhang, Multi-objective optimization strategy for regional multi-energy systems integrated with medium-high temperature solar thermal technology, *Energy* 300 (2024) 1–13.
- [10] L. T. Al-Bahrani, B. Horan, M. Seyedmahmoudian, A. Stojcevski, Dynamic economic emission dispatch with load demand management for the load demand of electric vehicles during crest shaving and valley filling in smart cities environment, *Energy* 195 (2020) 1–13.
- [11] H. Li, J. Liang, W. Han, X. Dai, Multifunctional power grid dispatching system based on electric vehicles cluster, in: *2022 7th Asia Conference on Power and Electrical Engineering (ACPEE)*, 2022.
- [12] P. A. Ostergaard, Comparing electricity, heat and biogas storages' impacts on renewable energy integration, *Energy* 37 (1) (2012) 255–262.
- [13] Y. Zhou, S. Chen, N. Han, J. Xiao, J. Xu, Research on load characteristics and demand response control model of river water source heat pump system, in: *2021 6th International Conference on Power and Renewable Energy (ICPRE)*, 2021.
- [14] X. Chen, S. Tao, Y. Sun, H. Wang, Y. Wang, J. Xing, Z. Liu, H. Xiang, Y. Liu, Research on optimal scheduling method of solar assisted heat pump drying system based on demand response, *Appl. Therm. Eng.* 243 (2024) 1–16.
- [15] Y. Cai, W. Chen, C. Zhang, Q. Ye, Z. Jiang, X. Liu, Analysis and research on the flexible load response ability of central air conditioning, in: *2023 IEEE Int. Conf. Energy Internet*, 2023, pp. 373–378.
- [16] M. Yue, H. Lambert, E. Pahon, R. Roche, S. Jemei, D. Hissel, Hydrogen energy systems: A critical review of technologies, applications, trends and challenges, *Renew. Sustain. Energy Rev.* 146 (2021) 1–21.
- [17] J. Hwang, K. Maharjan, H. Cho, A review of hydrogen utilization in power generation and transportation sectors: Achievements and future challenges, *Int. J. Hydrogen Energy* 48 (74) (2023) 28629–28648.
- [18] G. Leonzio, A. Hankin, N. Shah, CO₂ electrochemical reduction: A state-of-the-art review with economic and environmental analyses, *Chem. Eng. Res. Des.* 208 (2024) 934–955.
- [19] M. Bailera, S. Espatolero, P. Lisbona, L. M. Romeo, Power to gas-electrochemical industry hybrid systems: A case study, *Appl. Energ.* 202 (2017) 435–446.
- [20] X. Zhang, Y. Zhang, Environment-friendly and economical scheduling optimization for integrated energy system considering power-to-gas technology and carbon capture power plant, *J. Clean Prod.* 276 (2020) 1–16.
- [21] J. Lee, K. H. Ryu, J. H. Lee, Optimal design and evaluation of electrochemical CO₂ reduction system with renewable energy generation using two-stage stochastic programming, *J. CO₂ Util.* 61 (2022) 1–9.
- [22] Y. Li, C. Wang, G. Li, C. Chen, Optimal scheduling of integrated demand response-enabled integrated energy systems with uncertain renewable generations: A stackelberg game approach, *Energ. Convers. Manage.* 235 (2021) 1–11.
- [23] Z. Yang, M. Ni, H. Liu, Pricing strategy of multi-energy provider considering integrated demand response, *IEEE Access* 8 (2020) 149041–149051.
- [24] H. Tan, W. Yan, Z. Ren, Q. Wang, M. A. Mohamed, A robust dispatch model for integrated electricity and heat networks considering price-based integrated demand response, *Energy* 239 (2022) 1–12.
- [25] Y. Xi, J. Fang, Z. Chen, Q. Zeng, H. Lund, Optimal coordination of flexible resources in the gas-heat-electricity integrated energy system, *Energy* 223 (2021) 1–13.
- [26] S. Li, L. Zhang, X. Liu, C. Zhu, Collaborative operation optimization and benefit-sharing strategy of rural hybrid renewable energy systems based on a circular economy: A nash bargaining model, *Energy Convers. Manag.* 283 (2023) 1–21.
- [27] H. Wang, K. Li, C. Zhang, J. Chen, Capacity and operation joint optimization for integrated energy system based on nash bargaining game, *Energy* 305 (2024) 1–14.
- [28] Y. Huang, Y. Wang, N. Liu, Low-carbon economic dispatch and energy sharing method of multiple integrated energy systems from the perspective of system of systems, *Energy* 244 (2020) 1–18.
- [29] Y. Wang, J. Hu, N. Liu, Energy management in integrated energy system using energy-carbon integrated pricing method, *IEEE Trans. Sustainable Energy* 14 (4) (2023) 1992–2005.
- [30] J. Yang, B. Zhao, K. Ma, J. Zhong, W. Xu, A carbon integrated energy pricing strategy based on non-cooperative game for energy hub in seaport energy system, *Energy* 309 (2024) 1–12.
- [31] S. Ma, Y. Mi, S. Shi, D. Li, H. Xing, P. Wang, Low-carbon economic operation of energy hub integrated with linearization model and nodal energy-carbon price, *Energy* 294 (2024) 1–13.

- [32] R. Dai, X. Zhang, H. Zou, Two-stage distributed robust optimal allocation of integrated energy systems under carbon trading mechanism, *Processes* 12 (6) (2024) 1–17.
- [33] S. Guo, Y. He, H. Pei, S. Wu, The multi-objective capacity optimization of wind-photovoltaic-thermal energy storage hybrid power system with electric heater, *Sol. Energy* 195 (2020) 138–149.
- [34] H. Shen, H. Zhang, Y. Xu, H. Chen, Y. Zhu, Z. Zhang, W. Li, Multi-objective capacity configuration optimization of an integrated energy system considering economy and environment with harvest heat, *Energy Convers. Manag.* 269 (2022) 1–15.
- [35] J. Zhou, W. Zhang, Coal consumption prediction in thermal power units: A feature construction and selection method, *Energy* 273 (2023) 1–11.
- [36] D. Wu, S. Han, L. Wang, G. Li, J. Guo, Multi-parameter optimization design method for energy system in low-carbon park with integrated hybrid energy storage, *Energy Convers. Manag.* 291 (2023) 1–16.
- [37] D. M. Weekes, D. A. Salvatore, A. Reyes, A. Huang, C. P. Berlinguette, Electrolytic CO₂ reduction in a flow cell, *Acc. Chem. Res.* 51 (4) (2022) 910–918.
- [38] L. Zuo, Y. Deng, L. Chen, T. He, J. Yang, J. Zhang, Fundamental insights into photoelectrochemical carbon dioxide reduction: Elucidating the reaction pathways, *ACS Catal.* 14 (22) (2024) 16795–16833.
- [39] S. Jin, Z. Hao, K. Zhang, Z. Yan, J. Chen, Advances and challenges for the electrochemical reduction of CO₂ to CO: From fundamentals to industrialization, *Angew. Chemie Int. Ed.* 60 (38) (2021) 20627–20648.
- [40] T. Zheng, C. Liu, C. Guo, M. Zhang, X. Li, Q. Jiang, W. Xue, H. Li, A. Li, C.-W. Pao, J. Xiao, C. Xia, J. Zeng, Copper-catalysed exclusive CO₂ to pure formic acid conversion via single-atom alloying, *Nat. Nanotechnol.* 16 (12) (2021) 1386–1393.
- [41] S. Kong, X. Lv, X. Wang, Z. Liu, Z. Li, B. Jia, D. Sun, C. Yang, L. Liu, A. Guan, J. Wang, G. Zheng, F. Huang, Delocalization state-induced selective bond breaking for efficient methanol electrosynthesis from CO₂, *Nat. Catal.* 6 (1) (2023) 6–15.
- [42] L. Ding, N. Zhu, Y. Hu, Z. Chen, P. Song, T. Sheng, Z. Wu, Y. Xiong, Over 70% faradaic efficiency for CO₂ electroreduction to ethanol enabled by potassium dopant-tuned interaction between copper sites and intermediates, *Angew. Chemie Int. Ed.* 61 (36) (2022) 1–7.
- [43] W. Liu, P. Zhai, A. Li, B. Wei, K. Si, Y. Wei, X. Wang, G. Zhu, Q. Chen, X. Gu, R. Zhang, W. Zhou, Y. Gong, Electrochemical CO₂ reduction to ethylene by ultrathin CuO nanoplate arrays, *Nat. Commun.* 13 (1) (2022) 1–12.
- [44] G. Zeng, T. A. Pham, S. Vanka, G. Liu, C. Song, J. K. Cooper, Z. Mi, T. Ogitsu, F. M. Toma, Development of a photoelectrochemically self-improving Si/GaN photocathode for efficient and durable H₂ production, *Nat. Mater.* 20 (8) (2021) 1130–1135.
- [45] L. Yin, M. Tao, Correlational broad learning for optimal scheduling of integrated energy systems considering distributed ground source heat pump heat storage systems, *Energy* 239 (2022) 1–14.
- [46] Q. Zeng, J. Fang, J. Li, Z. Chen, Steady-state analysis of the integrated natural gas and electric power system with bi-directional energy conversion, *Appl. Energy* 184 (2016) 1483–1492.
- [47] J. Zheng, Z. Zhou, J. Zhao, J. Wang, Function method for dynamic temperature simulation of district heating network, *Appl. Therm. Eng.* 123 (2017) 682–688.
- [48] Y. Xi, T. Hamacher, V. Peric, Z. Chen, H. Lund, Bi-level programming for integrating flexible demand in combined smart energy system, in: 2021 IEEE Int. Smart Cities Conf., 2021, pp. 1–6.
- [49] M. J. Osborne, A. Rubinstein, *A course in game theory*, MIT Press, 1994.
- [50] A. Pfeifer, F. Feijoo, N. Duić, Fast energy transition as a best strategy for all? the nash equilibrium of long-term energy planning strategies in coupled power markets, *Energy* 284 (2023) 1–12.
- [51] A. Granas, J. Dugundji, *Fixed Point Theory*, New York: Springer, 2003.
- [52] F. Meng, X. J. Zeng, Y. Zhang, C. J. Dent, D. Gong, An integrated optimization + learning approach to optimal dynamic pricing for the retailer with multi-type customers in smart grids, *Inf. Sci. (Ny)*. 448-449 (2018) 215–232.
- [53] H. Wang, C. Zhang, K. Li, S. Liu, S. Li, Y. Wang, Distributed coordinative transaction of a community integrated energy system based on a tri-level game model, *Appl. Energy* 295 (2021) 1–13.
- [54] J. Fang, Q. Zeng, X. Ai, Z. Chen, J. Wen, Dynamic optimal energy flow in the integrated natural gas and electrical power systems, *IEEE Trans. Sustain. Energy* 9 (1) (2018) 188–198.